Report 1989

Section for inorganic chemistry
Department of Chemistry
University of Oslo
Norway

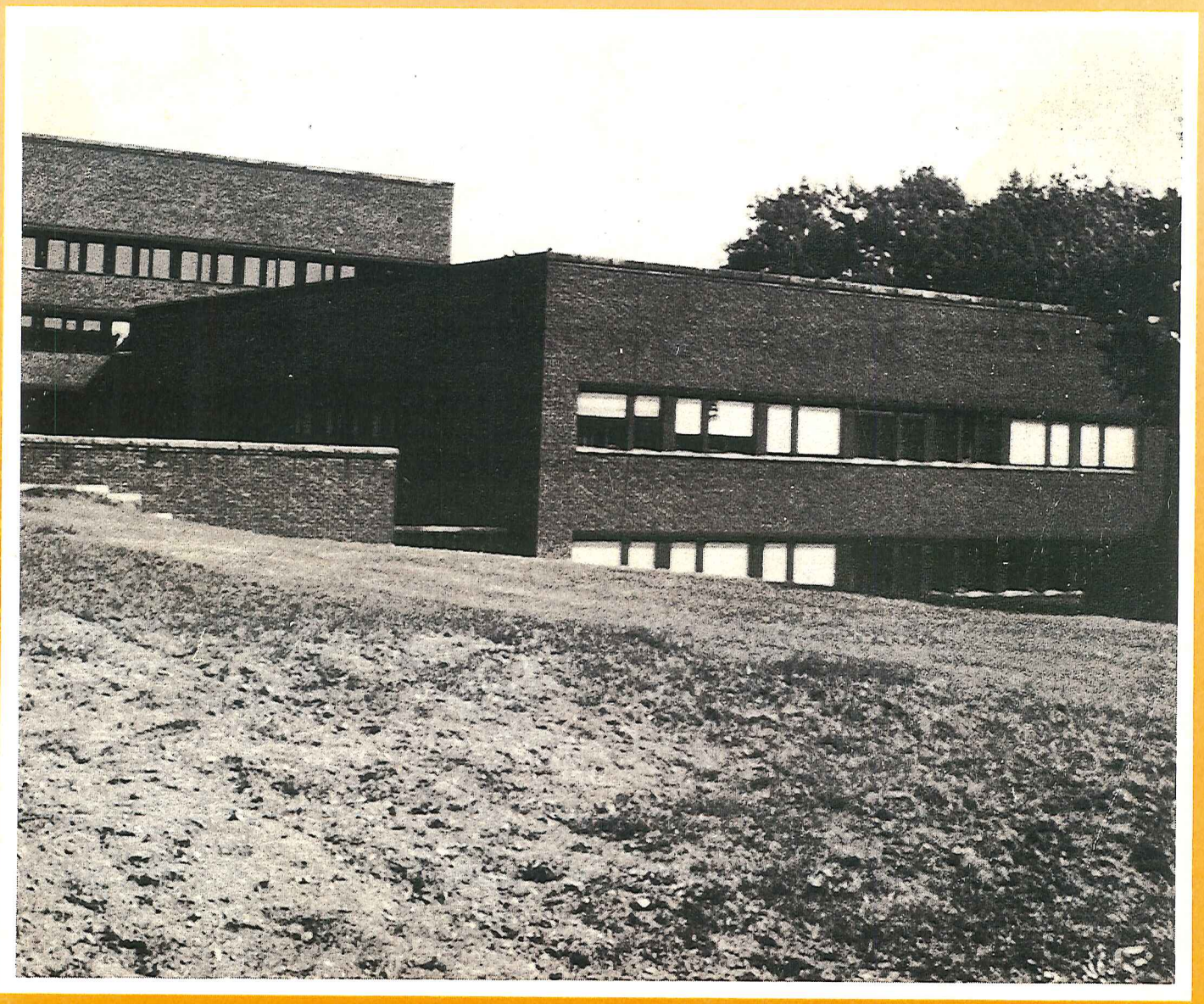

Report 1989

Section for inorganic chemistry
Department of Chemistry
University of Oslo
Norway

Editors

Espen Bergsmark
Arve Holt

Oslo, August 1990

Preface

The Section for inorganic chemistry at the Department of Chemistry, University of Oslo, is this year taking up the old tradition of presenting a yearly report. However, regularly all activities at the Department of Chemistry have been presented together with publication lists in the report series "Navn og tall". The Section now considers the research activities in inorganic chemistry and material science to be so broad that they deserve a more thorough presentation.

The different parts of this report put emphasis on research programs, teaching and organization of the Section. A rather broad description of all activities are first given, followed by a few examples of scientific results obtained during the academic year of 1989. The list of publications is supplemented by abtracts for the various articles, thereby providing the interested reader some insight into the topics.

Of the altogether 41 people at the Section, there are 9 Dr. scient. and 11 Cand. scient. students. We are happy to register that inorganic chemistry and material science has become increasingly more popular among the students. The number of students in these areas has constantly increased during the last few years although there has been a decline of students in chemistry as a whole.

Inorganic chemistry, in a broad sense, forms an important basis for the understandig of material properties and processes relevant to most of the traditional Norwegian industry. Another challenge for this part of chemistry is to engage in international collaboration. In this respect, the use of advanced methods, e.g. based on neutron and synchrotron radiation, at large multinational facilities, as well as collaboration with foreign universitites are important for our activities.

We want to thank our main external sponsors for providing financial support for equipment, fellowships and running project costs. In particular, our thanks go to the Norwegian Research Council for Science and the Humanities (NAVF) and the Royal Norwegian Council for Scientific and Industrial Research (NTNF). Finally, thanks go to those who directly or indirectly have contributed to make this yearly report possible.

Helmer Fjellvåg
(section head)

Contents:

The Section for Inorganic Chemistry

The Section for inorganic chemistry is one out of five sections at the Department of Chemistry, University of Oslo, with altogether 41 people, including teachers in permanent and temporary positions, technicians, fellowship holders and students. The aim of this yearly report is to provide information on how our total resources are used, mainly with respect to research efforts but also including remarks concerning teaching and administration. The activity of the Section is teaching and research.

During the last decade materials science has been taken up by the Faculty of Mathematics and Natural Sciences, and the teaching of relevant subjects are done by this Section at the Department of Chemistry and by different groups at the Department of Physics. The research activities at the Section comprise basic research in inorganic chemistry, particularly chemistry of solids, and materials science. Part of the projects are oriented towards future applications in cooperation with institutes for sponsored research and industry. The major aim of the research activities is to educate graduate students (cand. scient. and dr. scient.) and to produce high quality research. The results are generally published in international journals and presented at national and international conferences. In selected areas the section aims at having competence of high international quality.

The Section is involved in a large number of research programmes involving other Norwegian research institutes, Norwegian companies and laboratories and universities abroad. A list of research partners outside the University of Oslo are given on page 32. The Section has a wide range of international contacts, probably these are just as well developed as the the national ones.

At the Section, the researchers are engaged in a wide range of topics, mainly concerning the solid state. Formally, the Section consists of two research groups; one in electrochemistry, and one in inorganic chemistry and material science. However, the real situation is different, in particular for the latter group, as will be evident from the following parts of this report. Instead of subdividing the personnel into rigid groups, the research is, when suitable, based on collaboration between different members of the Section.

Studies of structure–property relations in general require the use of several methods. A large part of the research at the Section is problem-oriented. The Section is reasonably well-equipped, and is within some areas the leading laboratory in Norway. In particular, equipment for powder diffractions studies, measurements of magnetic properties, determination of heat capacity at high temperatures, corrosion and for studies of surfaces by microscopy techniques may be mentioned.

In October 1989 Dr. techn. Ketil Videm was employed as professor in the vacant position after professor Tor Hurlen, who now has a professorship payed by the NAVF. Concerning the future, the age distribution at the Section as well as at the Department of chemistry calls for concern, e.g. training of possible new staff members. This is a problem taken seriously by the Section, since in general there are too few people prepared to enter permanent positions in the fields of condensed matter physics, solid state chemistry, inorganic chemistry and material science. However, this is not only a question of qualifications, resources and research possibilities. Salaries, benefits, and good working conditions play a more and more important role for young scientists choosing a future employment.

Research at the Section of inorganic chemistry

In the next chapter, a few detailed examples from our research activities are given. However, they represent just a part of our total

activity. Thus, a short general description is given here.

The research group for electrochemistry has two staff members, Ketil Videm and Tor Hurlen (see above). There are three doctor students and two graduate students in the group. The activities are directed towards passive behaviour of various metals in aqueous solutions. Attention is paid to the formation, growth and breakdown of passive films as well as to the protecting properties of such films. Also phenomena like electron transfer and space charge distribution are studied. The metals and their chemical environment are selected so that the fundamental understanding gained may be useful for practical applications.

The research group for inorganic chemistry and material science (with altogether 8 staff members, 8 technicians, and 9 fellowship holders, 6 dr. scient. and 9 cand. scient. students) is covering a wide range of activities and using heavily a large number of methods. One specific activity is the study of thermodynamic properties of inorganic solids. In addition to the two staff members specialized in this field, Fredrik Grønvold and Sven R. Svendsen, there are also other activities where emphasis is put on obtaining thermodynamic data.

The Section has equipment for obtaining accurate heat capacity data at high temperatures, i.e. 273–1000 K. Such data are obtained for several inorganic compounds and materials of technological applications. Examples can be the Cu–S system fast ionic conductors and cristoballite. Complementary low-temperature data are obtained in collaboration with E. F. Westrum Jr., Ann Arbor, U.S.A. Another topic within thermodynamics, is the study of vapour pressures of transition metal chalcogenides.

Per Kofstad is heading an activity on high temperature corrosion (gas–metal reactions) which comprises studies under various conditions, e.g. in gaseous environments such as $CO + CO_2$, $CH_4 + H_2$ and $SO_2 + O_2$, and effects of layers of molten salt on metal surfaces. The experimental studies comprise measurements of reaction kinetics by means of thermogravimetry and characterization of reacted specimens by metallography, X-ray diffraction, scanning electron microscopy, scanning Auger spectroscopy, etc.

Metal oxides and other ceramic materials are subject of extensive investigations at the Section by two different constellations of collaborating scientists. They comprise structural studies, nonstoichiometry, defect structures, transport properties, and catalytic properties.

The first group, Per Kofstad and Truls Norby (temporary position) are studying defects and defect-dependent properties of oxides at high temperatures (> 500 °C). Of particular interest are studies of hydrogen defects in the form of dissolved protons in metal oxides. Defect structures of oxides are particularly studied through measurements of transport properties such as electrical conductivity (impedance spectroscopy). The use of such studies in the development of fuel cells and electrochemical reactors are further described below.

The second group, Helmer Fjellvåg, Arne Kjekshus and Pavel Karen (temporary position), concentrates on the relation between atomic arrangement, chemical substitution and physical properties. Of particular interest are superconducting high-T_c oxides, and perovskite related phases in general.

The crystal structure of zeolites, dehydrated, with template or organic molecules in the channels/cages are studied by diffraction and n.m.r. methods. Carbides of Mn and Mg represent another topic attacked by powder diffraction methods (see also p. 10). The traditional field of studies of phosphides and arsenides of the d-metals is continued, inter alia by elucidating complex magnetic phase diagrams and considering multicritical points in temperature – pressure (or chemical pressure, viz. substitution) diagrams. The cooperation on neutron scattering with the Institute for Energy Technology is still important, although experiments are also done abroad.

Ternary systems, either solely between d-metals, or including one or two non-metals

from the main groups IV, V and VI are studied. Metallization of GaAs by Ni is one such example. Sigrid Furuseth is studying several Ni-group IV, V systems, Trond Rakke devotes his interst to those phases having dumbell pairs of non-metal atoms (pyrites, marcasites, etc.) and Erling Røst studies typical alloy systems like Au–Cu–Sn.

Projects are also run on typical low-dimensional systems (Sigrid Furuseth and others), ranging from synthesis of new phases, via structure determination to intercalation. Finally, it should be mentioned that one reason behind the success of the Section within various fields of solid state chemistry, is the skill on how to synthesize pure, high-quality samples of quite different materials.

Outlook for future research

Two staff members, Kofstad and Videm, will from about May 1990 together with some fellowship holders and students, move a large part of their activities to the Center for Materials Research in the Research Park at the University of Oslo. However, the large part of material science, and in particular the basic aspects, will still be located at the Department of chemistry itself. The aim is, within selected areas, to create new cooperation with industrial firms in the Research Park. The activities in the Research Park will cover aspects connected with fuel cells and corrosion of metals in various atmospheres or in aqeous solutions.

The Section has recently obtained new and advanced equipment for the study of electronic properties of surfaces by XPS and scanning Auger microscopy (SAM). Another important tool obtained in 1989 is a SQUID magnetometer for detailed studies of magnetic properties. These two instruments will definitely be important in future research at the Section. The Auger/XPS instrument will be moved to the Research Park during 1990.

On the international scene, the availibility of synchrotron radiation (SR), will have a large impact on the study of condensed matter. The Norwegian part of the European Synchrotron Radiation Facility, ESRF, in Grenoble, is limited to 0.56%. The source will be operative first by 1994, however, already now the NAVF has set up a program so that research groups can gain knowledge on how to use the various SR-based methods for studies in chemistry, physics and material science. In this context, the Section aims at obtaining a central position for SR-based research in the Oslo-region (material science crystallography, EXAFS).

Teaching at the Section for inorganic chemistry

The teaching duties of the staff is within inorganic chemistry and material science. In addition, the staff also contribute in teaching the first course in general chemistry. In addition to the normal staff members, those fellowship holders payed by the University have teaching duties.

Each chemistry student passes the basic course in inorganic chemistry (KJ110) during his/her first/second year at the university. The next encounter with inorganic chemistry is about one year later when students starts to spesialize. Our students then attend courses either in Inorganic chemistry II (KJ211), Inorganic chemistry III (KJ212), Analyses of condensed materials (KJ213), Material science (MVT200) or Corrosion of metals (MVT202). For the graduate and doctorate students, courses are given in Solid state chemistry (KJ316), Solid state reactions (KJ317) and Solid state thermodynamics (KJ319).

❑

New equipment:

The Auger/XPS instrument

In 1988, a grant from the Royal Norwegian Council for Science and Technology (NTNF) enabled the installation of a combined Auger-/XPS surface analysis instrument (Micro-Lab–3, VG Scientific Ltd, England) at the Department of Chemistry, University of Oslo (Fig. 1). The instrument is owned and used in partnership with Center for Industrial Research (SI) to serve the needs for surface analysis at the University and in industry. It is provisionally located at the Section of Inorganic Chemistry at the University, but will in 1990 be moved to the Center of Materials Research in the new Research Park at Blindern, Oslo.

Auger Electron Spectroscopy (AES) and Scanning Auger Microscopy (SAM)

Auger Electron Spectroscopy is based on interaction between energy levels in the atomic electron shell. A preselected area of the surface to be analyzed is irradiated by a scan-

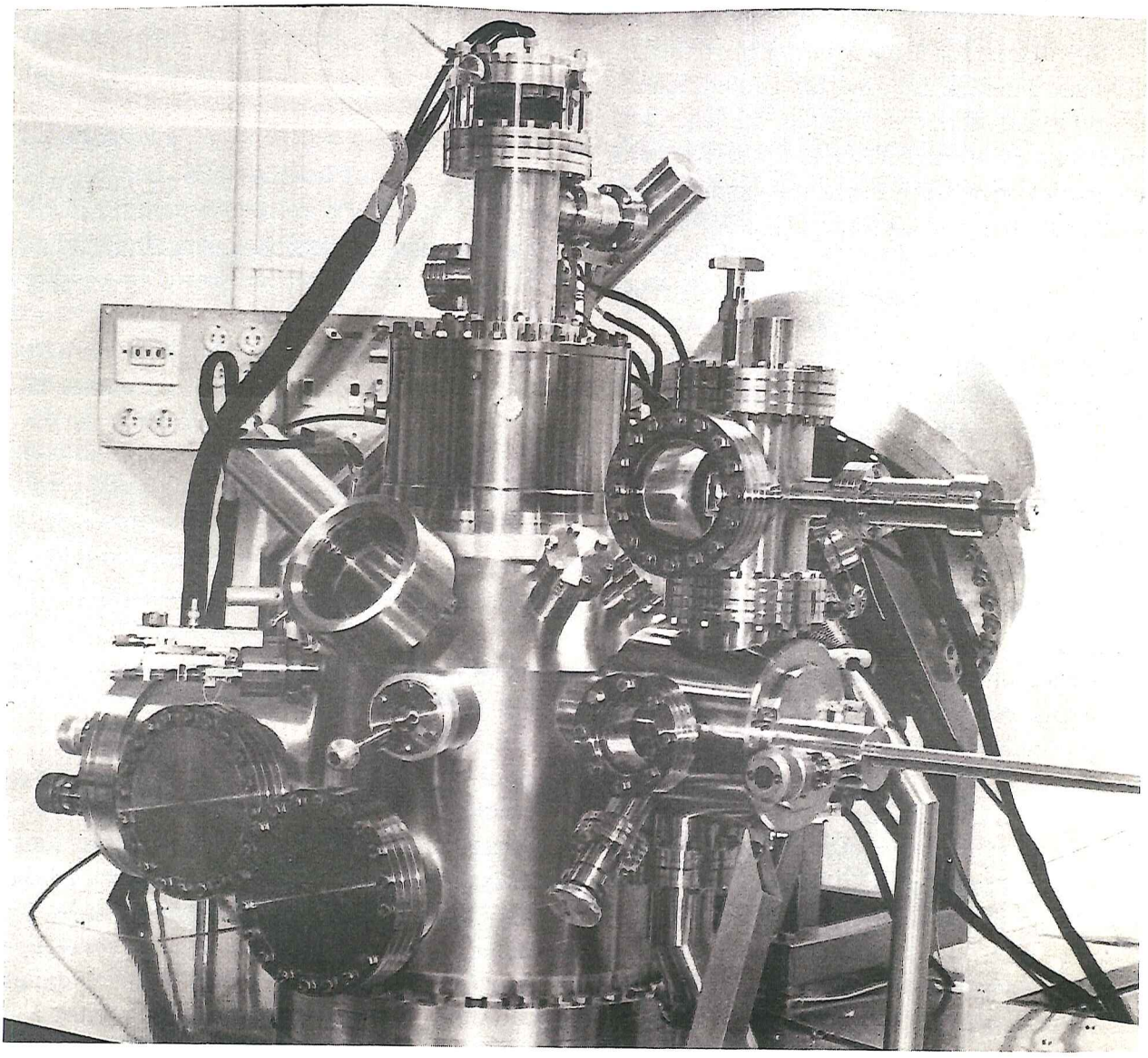

Fig. 1. The Auger/XPS instrument.

ning, low-energy electron beam. An incident electron may knock out an electron from an inner level of a target atom. The ionized atom may relax by filling the empty level through a transition from an outer level. To maintain the energy balance, an electron (called an Auger electron) from the same, or a more shallow level, is ejected. Auger electrons have characteristic energies dependent on the atomic number, the transition involved, and the chemical bonding of the excited atoms. The emitted Auger electrons are counted in an energy- discriminating hemispherical analyzer, and an energy spectrum is thus obtained. The low-energetic Auger electrons can escape only through a few atom layers, and the effective analysis depth is thus around 2 nanometers.

In Auger Electron Spectroscopy (AES), the peak energies are used for element identification and determination of the chemical environment of the surface species. The peak intensities reveal the elemental composition, ideally with a sensitivity of 0.1 atom-% of a monolayer.

In Scanning Auger Microscopy (SAM), an energy peak in the Auger spectrum is routed from the analyzer to a video monitor synchronized with the scanning incident electron beam. The specimen surface is thus mapped with respect to elemental composition. The lateral resolution is 50 nanometers, enabling analysis of, for instance, small particles and cross-sections of grain boundaries.

The high surface sensitivity of Auger and XPS methods necessitates operation under conditions where the accumulation rate of surface contaminants is negligible. T

he major contamination source is the residual gas in the vacuum system, generally requiring a vacuum better than 10^{-10} torr. The main restriction of AES/SAM is connected with the problem of charge buildup during analysis of non-conductive materials.

X-Ray Photoelectron Spectroscopy (XPS)

In XPS (also called ESCA), the specimen surface is irradiated with soft Kα X-rays from an

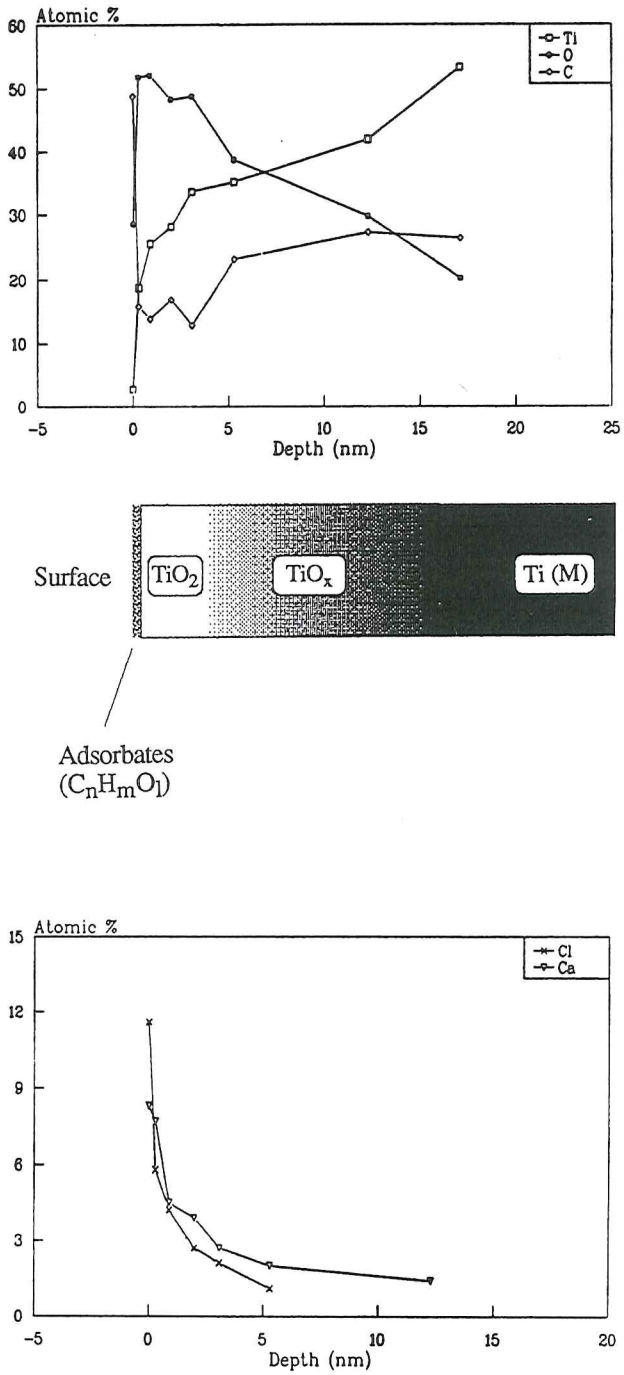

Fig. 2. Depth profiles of $CaCl_2$-treated Ti-metal.

Al or Mg source. This leads to a continuous escape of photoelectrons from the upper 2–3 nanometers. These are counted in the same analyzer as used for Auger electrons, and the XPS spectrum can accordingly be used for element identification and quantitative analysis. 'Chemical shifts' in the peak energies may be used to identify oxidation states and chemical environment of surface species.

XPS can be applied to non-conducting materials, but the lateral resolution is limited to around 0.3 mm, mainly due to the use of an unfocused incident X-ray beam.

Depth profiling

During depth profiling, argon gas is ionized to Ar^+ ions and accelerated towards the specimen. The ion gun can focus the beam and raster it across a selected area of the surface. The heavy argon ions sputter away surface species and causes gradual removal of atomic layers. By alternate analysis (AES or XPS) and sputtering, it is possible to study the change in elemental composition and chemical environment as a function of distance from the original surface, ideally with a resolution of one monolayer. The maximum profiling depth is typically one micrometer, limited by the capacity of the ion gun.

Applications

The methods as described above are suitable for examining properties and processes such as contamination, adsorption, catalysis, oxidation and corrosion, passivation, interdiffusion, coatings, etc. In the first one and a half years of service the instrument has been used for studying, for instance, metals (corrosion layers), ceramics (interdiffusion in fuel cell materials) and polymers (surface composition). The following is an example of an XPS study done in 1989 for the Faculty of Odontology, University of Oslo.

An example: Titanium metal in dental implant technology

Titanium metal (Ti) is a promising candidate for many dental applications, being non-toxic, light, and strong. It is very corrosion-resistant thanks to a protective oxide layer of TiO_2. The ability of Ti metal to make a strong bond to bone may be related to chemical interactions between calcium (Ca) in the bone tissue of teeth and the TiO_2 layer on the titanium implants.

In a first study of these processes, one decided to look at the behaviour of TiO_2 in a $CaCl_2$ solution, and to examine the resulting distribution of Ca (and Cl) in TiO_2. In one of the experiments, a Ti tablet was treated in 0.3 M $CaCl_2$ and washed in destilled water. An XPS depth profile was done for the following elements: Ti, O, C, Ca and Cl. The profiles are shown in Fig. 2. In the outer few nanometers, a thin film of organic adsorbates could be recognized. This visualizes the high sensitivity of XPS to contaminant overlayers. Underneath the organic film, the Ti metal is covered with a layer of TiO_2, contaminated with organic species (C, Fig. 2). Between the TiO_2 and Ti metal is a region of reduced oxides, possibly with layers of lower oxides such as Ti_2O_3 and TiO. The total oxide thickness is around 13 nanometers. Figure 2 shows that a small content of Ca and Cl was found only in the outermost atom layers of the TiO_2.

Ingvild Lorentzen

The solving of old problems in inorganic chemistry by means of powder diffraction techniques

A quite astonishing fact is that the crystal structures of some of the compounds one learned about in the first course of inorganic chemistry in reality still are unknown. Two such examples were until recently provided by I_2O_4 and Mg_2C_3. The former compound was actually well-characterized already in 1844. Recent advances in powder diffraction techniques (resolution, flux, and computer programs) and in particular the combined use of X-ray and neutron diffraction, has opened up for solving old structural problems. For most compounds, one can obtain single crystals so that the structure can be solved by common single crystal methods. However, some compounds do not easily form larger crystals. In the case of I_2O_4 low thermal stability (decomposition into I_2O_5 and I_2) and no known recrystallization solvent prevents crystal growth. Also the route of synthesis by thermal decomposition of $(IO)_2{\cdot}SO_4$ just provide powders of small particle size. For Mg_2C_3, the high reactivity makes single crystal growth experiments cumbersome. This means that in both cases powder diffraction methods must be used in the process of solving and refining the structure. An example of a powder X-ray diffraction diagram obtained by synchrotron radiation at Hasylab, Hamburg, is given for I_2O_4 in Fig. 1.

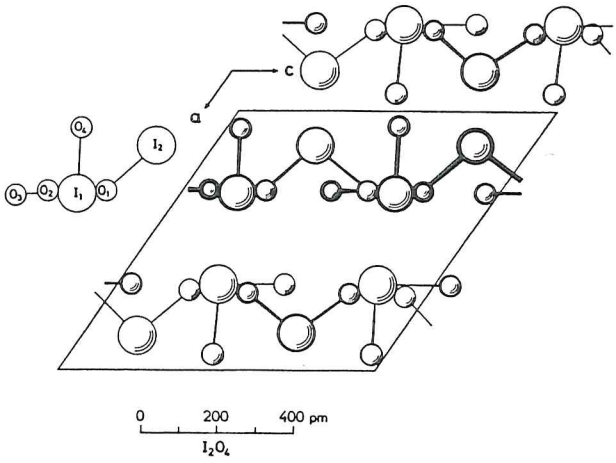

Fig. 2. Projection of the crystal structure of I_2O_4 on the ac-plane.

The procedure for solving these problems involve the steps:

(i) Define the unit cell by means of trial and error indexing of either Guinier film data or diffractometer data using synchrotron radiation.

(ii) Extract structure factors (integrated intensities) from observed powder X-ray diffraction profiles by deconvolution refinements.

(iii) Locate the "heavy" atom with respect to X-rays (here, iodine and magnesium, respectively) using e.g. Patterson methods.

(iv) Locate the remaining atoms by difference Fourier maps.

(v) Confirm the structure by Rietveld (profile) refinement of the powder neutron (and X-ray) diffraction data.

For the solving of the structure, both for I_2O_4 and Mg_2C_3, the combined use of

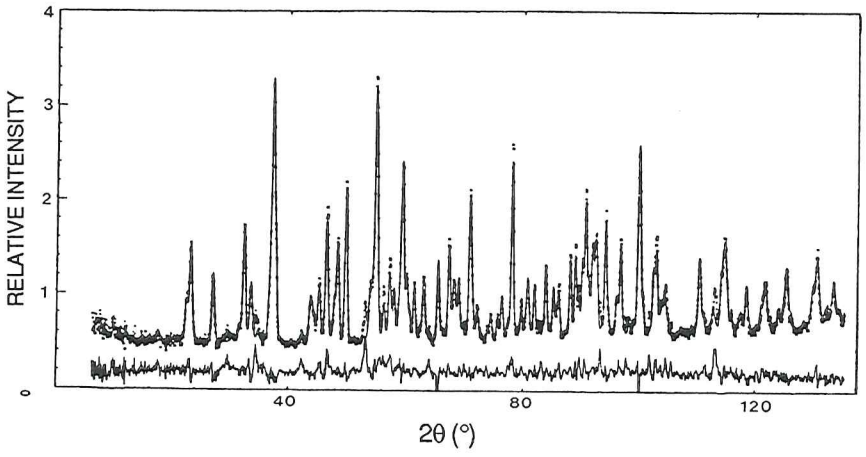

Fig. 1. Powder X-ray diffraction diagram of I_2O_4 collected at the Wiggler station at Hasylab, Hamburg; wavelength 1.3917 Å. (Observed, calculated and difference intensities are shown.)

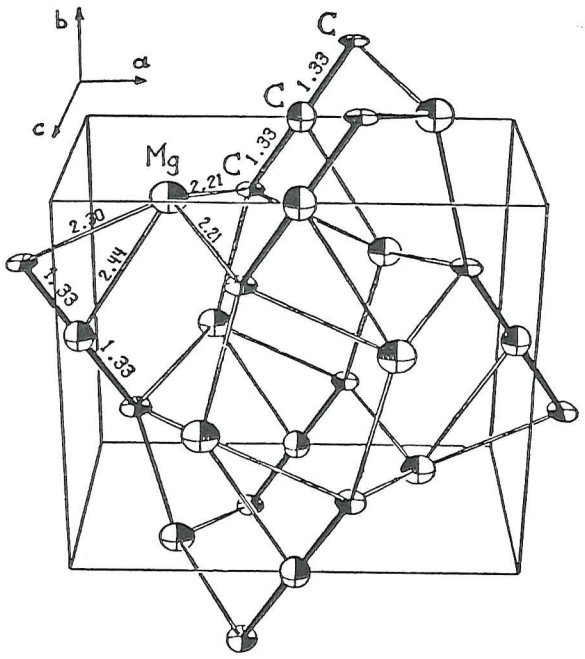

Fig. 3. The crystal structure of Mg_2C_3.

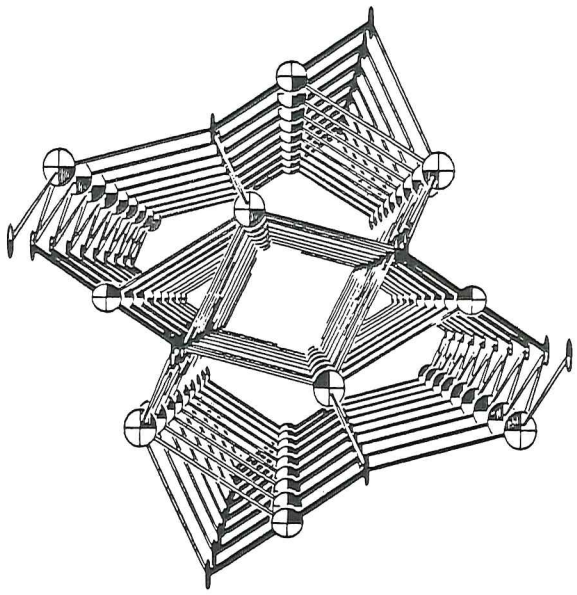

Fig. 4. ORTEP-plot of segment of the crystal structure of Mg_2C_3.

X-rays and neutrons is extremely helpful. With respect to X-rays, e.g. oxygen scatters only a fraction of what iodine does, but with respect to neutrons oxygen is actually the stronger scatterer of these elements. Similar features, although less enhanced, applies for the pair of elements Mg and C.

In various steps of the calculations, the programs TREOR, CELLKANT, GX, XRS82, ALLHKL and EDINP are used.

The crystal structures of I_2O_4 and Mg_2C_3 are shown in Figs. 2 and 3. I_2O_4 (space group P21/c) is seen to be an almost completely one dimensional solid. The chains, described as [–I–O–IO_2–O–]n, run parallel to the c-axis, see Fig. 2. The chains are stacked together at distances slightly shorter than expected from van der Waals radii. Considering the interatomic distances, I_2O_4 shows a slight tendency to be build by polymerization of IO_2 units rather than to consist of IO and IO_3 building units. I_2O_4 show structural resemblance to $(IO)_2{\cdot}SO_4$ and I_2O_5, which respectively are the precursor and decomposition product in the synthesis-degradation process.

Among the large group of carbides, Mg_2C_3 is positioned in the border region between the ionic and covalent (metallic) carbides, cf. e.g. the electronegativity of the metal component. Mg_2C_3 constitutes the first example of a carbide having C3-groups. The C34-unit is isoelectronic to CO_2 and has linear geometry, see Figs. 3 and 4. The C–C distance of 133 pm is slightly longer than in allene (131 pm) which probably is due to bridging effects (polycenter bonds) of the surrounding Mg atoms. In the more ionic dicarbides the C–C distance is about 120 pm. Mg_2C_3 can to some degree be considered as a magnesiocarbon.

The future of powder diffraction will definitely be very fruitful. There is certainly a limit for the complexity of structures which may be attacked by ab initio procedures. However, when considering the enormous improvement foreseen in powder diffraction when e.g. the European Synchrotron Radiation Facility in Grenoble will become operative at the middle of the nineties, rather complicated problems can be solved, probably for unit cells containing as much as 40 atoms in the asymmetric unit.

Helmer Fjellvåg

The effect of substitution on the physical properties of the high temperature superconductor $YBa_2Cu_3O_{9-\delta}$, examplified by La for Ba substitution

Since the discovery in 1987 of the high T_c phase $YBa_2Cu_3O_{9-\delta}$ (in scientific jargon YBCO or 123), scientists throughout the world are investing huge efforts into improving the superconducting characteristics of oxide based materials. Another purpose of these intense studies is to obtain experimental support for theoriticians in their struggle for developing a new theory which could explain T_c´s higher than some 35 K, which earlier was considered as the theoretical limit.

For solids, a close connection between structural and physical properties generally exists. For the mixed valency oxide $YBa_2Cu_3O_{9-\delta}$ correlations between features of the crystal structure and superconducting properties like T_c, the critical current, the critical magnetic field, and magnitude of the diamagnetic field repulsion are of interest.

$YBa_2Cu_3O_{9-\delta}$ has a homogeneity region ranging between $2.03 \leq \delta \leq 3$, over which the low-temperature transport properties changes from superconducting to semiconducting. At the same time, the formal copper valency varies between 2.31 and 1.67. The four different metal sites of the ordered, defect triple perovskite type structure, can each be the scene for a solid substitutional process. Candidates for substituents are selected according to valency, ionic radii and preferance for coordination polyhedra. The manipulation of the compositions are principally of two different types; (i) with keeping the formal valency of copper constant and (ii) with simultaneously changing the formal copper valency. The first way can be achieved by e.g.

– substitution of Y by some other trivalent rare earth element

– substitution of Ba by Sr (or another large divalent element)

– introduction of aliovalent substituents which automatically is fully compensated for in the oxygen content δ.

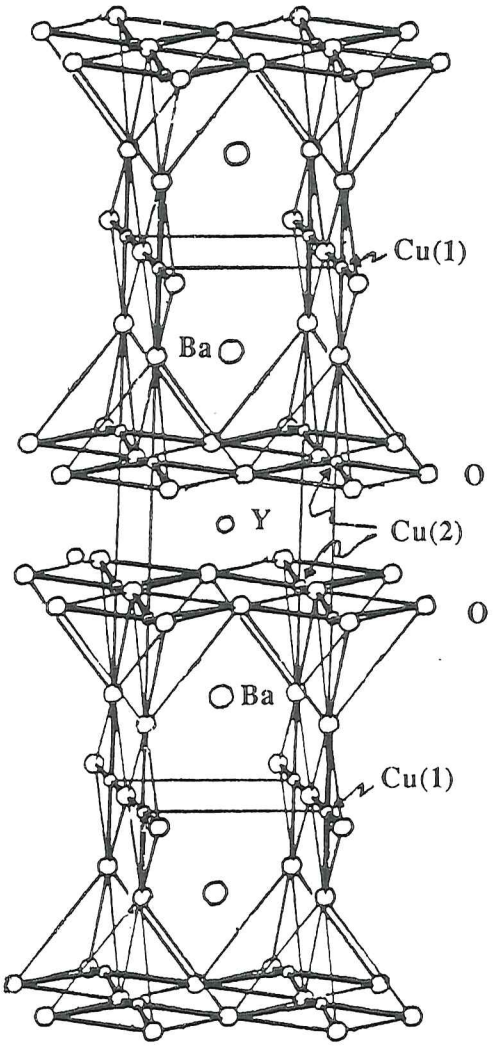

Fig. 1. Crystal structure of $YBa_2Cu_3O_{9-\delta}$.

The second way can be achieved by e.g.

– changing the oxygen content (cf. homogeneity region)

– introduction of aliovalent substituents without or with just partly compensating the oxygen content.

An interesting example which provides both options, is the substitution of Ba^{2+} by La^{3+}. Considering ionic radii, La^{3+} is smaller than

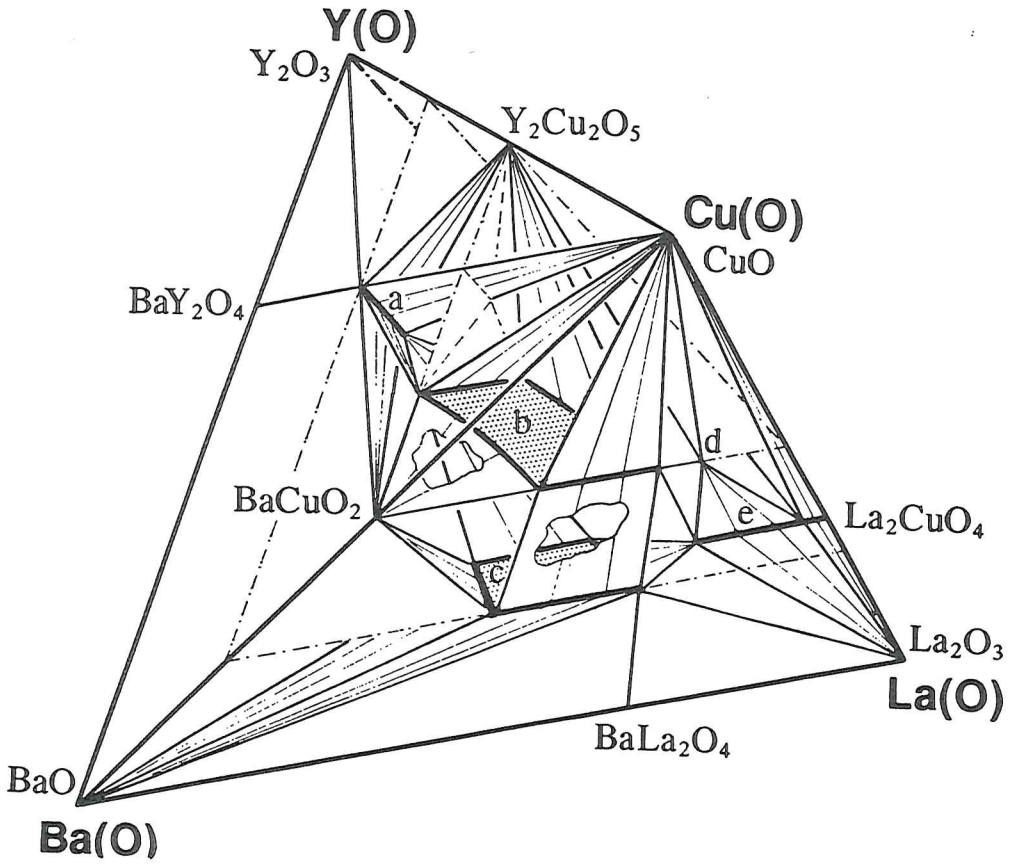

Fig. 2. Schematic tetrahedral phase diagram for the Y–La–Ba–Cu–(O) system.

Ba^{2+} but larger than Y^{3+}. This actually causes the substitution process to be very complex since lanthanum can substitute for yttrium as well as for barium. However, it is possible, selectively to produce samples belonging to the solid solution phase $Y(Ba_{1-y}La_y)_2Cu_3O_{9-\delta}$, with $0.00 \leq y \leq 0.35$ and $1.7 \leq \delta \leq 3.1$. The complex phase diagram is illustrated in Fig. 2.

The orthorhombic (ORT) crystal structure of $YBa_2Cu_3O_{9-\delta}$, see Fig. 1, may obtain tetragonal (TET) symmetry for certain composition (substitution) and temperature conditions. The main factor governing orthorhombicity is the uneven distribution of oxygen (O5) over possibly equivalent sites within the ab-plane running through 1/3 of the Cu-atoms, cf. Fig. 1. Increased La-content reduces the orthorhombic distortion due to increased oxygen content introduced via the higher valent lanthanum. The structure then turns tetragonal for $y > 0.14$ (at 300 K). The regions of ORT and TET phases as function of δ, y is shown in Fig. 3.

For e.g. $y = 0.15$, the peculiar phase transition sequence TET–ORT–TET takes place upon heating. This can also be understood by solely considering the O5 sites. Some of the originally 1.13 oxygens randomly distributed in the TET phase, are thermally removed and the 0, 1/2, 0 site becomes preferrably filled whereas 1/2, 0, 0 is emptied in the ORT phase, before continued heating and oxygen removal randomnizes the remaining oxygens (TET phase).

For oxygen saturated $Y(Ba_{1-y}La_y)_2Cu_3O_{9-\delta}$ the mixed formal copper valency of 2.31 stays constant. One main effect of introducing smaller La-atoms is hence to compress the unit cell and to act as a source of positive chemical pressure. The compression is anisotropic, being largest along the c-axis. The atomic arrangement relaxes via slight shifts in the positon parameters for atoms with unconstrained coordinates. In Fig. 4 is shown the variation of Tc with increasing La-content y.

For samples of $Y(Ba_{1-y}La_y)_2Cu_3O_{9-\delta}$

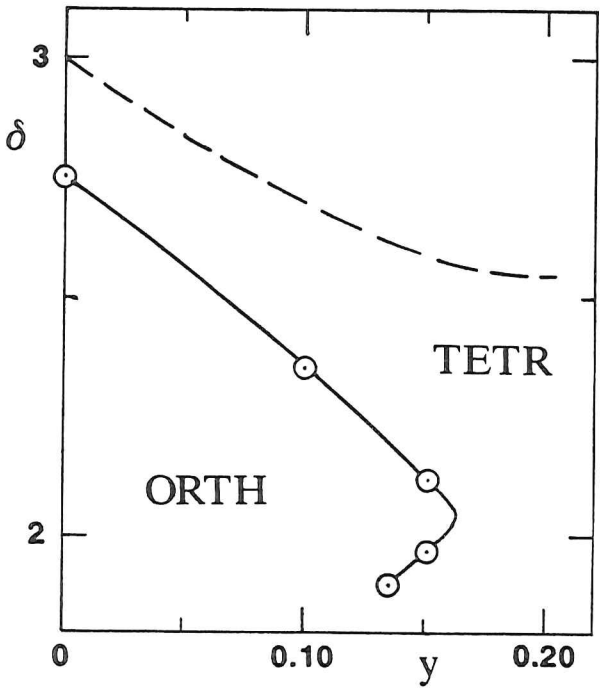

Fig. 3. Phase diagram showing existence range for orthorhombic and tetragonal phases as function of oxygen content and La-substitution.

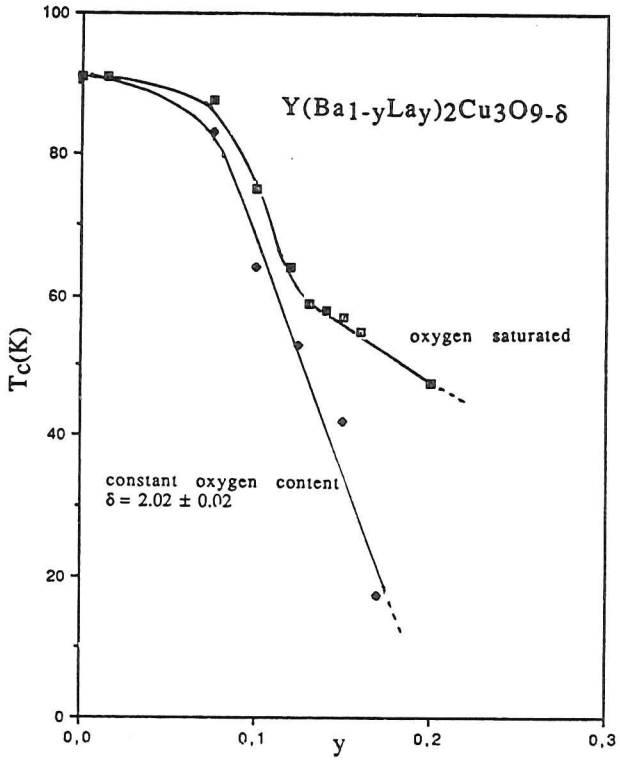

Fig. 4. Tc versus y for various samples of $Y(Ba_{1-y}La_y)_2Cu_3O_{9-\delta}$.

with constant oxygen content given by δ = 2.02 ±0.02, the formal valency of copper is continuously reduced from 2.31 for y = 0.00 to 2.11 for y = 0.30. In different words, the concentration of hole charge carriers is reduced. At the same time, La-substitution causes the structure to be anisotropically compressed. The variation of T_c with y is included in Fig. 4.

In order to account for the significant difference in the $T_c(y)$ behaviour (Fig. 4) for samples with respectively constant copper valency and constant oxygen content, at least two aspects have to be considered; first, the influence of the concentration of hole carriers on the superconductivity, and second, the change in electronic band structure brought about by the anisotropic lattice contraction. Belonging to the latter category, a clear correlation has been found between the reduction in the tetragonal deformation of the $Cu(2)O_5$ pyramid and the suppression of T_c.

Helmer Fjellvåg

Solid Oxide Fuel Cells and Electrochemical Reactors

Natural gas (methane) is generally converted to electrical energy in turbine/generator systems with limited efficiency. Burning methane with air in this way rises the dilemma that efficiency calls for a high temperature (the Carnot cycle), while a high flame temperature favors the formation of pollutants such as nitrogen oxides (NO_x).

Solid oxide fuel cells (SOFC) offer the possibility of converting methane into electrical energy in a direct, efficient high-temperature process. Fuel and the oxidant are not in direct contact, there is no flame, and the yield of pollutants is low.

The most common SOFC electrolyte is yttria-stabilized zirconia (YSZ), which is an oxygen ion conductor at high temperatures: Oxygen at the air electrode (cathode) is ionized to oxygen ions; these migrate through the electrolyte, react with the fuel at the anode, and give away electrons which do electrical work as they flow in an external circuit (Fig. 1).

The product at the fuel side may vary, as illustrated in Fig. 1, depending on the degree of oxidation, temperature, pressure, and catalytic properties of the anode. When full oxidation is accomplished, the products are CO_2 and H_2O, and all the chemical energy is utilized; we have a normal fuel cell. With a lower degree of oxidation, the products may be, for instance, higher hydrocarbons or methanol, and the cell is called an electrochemical reactor. Methane is here converted to more valuable chemicals, while the electrical output is lower than in fuel cells.

The University of Oslo collaborates with The Center for Industrial Research (SI) and the Norwegian Institute of Technology (NTH) in two projects on SOFCs with natural gas as fuel: The NORCELL project aims at the development of a prototype SOFC for production of electrical energy, while the SPUNG project aims at conversion to more valuable chemicals. Both projects are funded

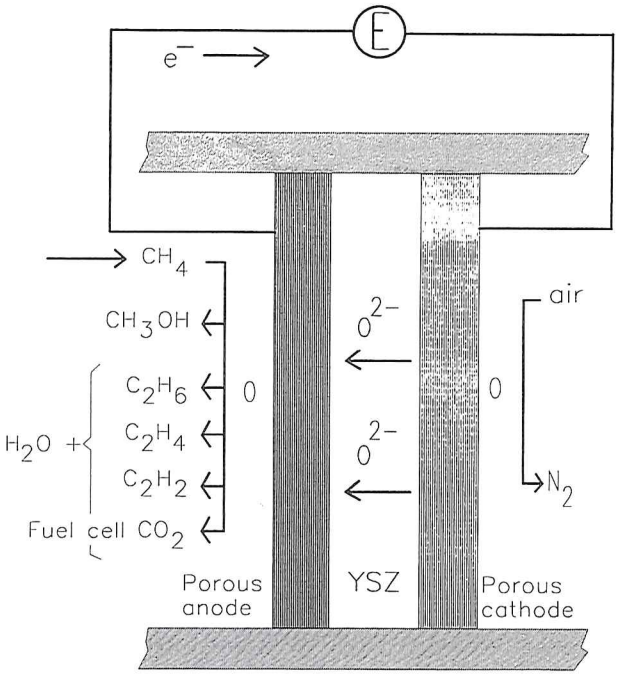

Fig.1. Partial or full oxidation of methane in an electrochemical cell with solid oxide electrolyte.

by the Royal Norwegian Council for Scientific and Industrial Research (NTNF) and Norwegian companies.

Professor Per Kofstad's group at the University of Oslo takes part in many aspects of the research on both projects, but the main effort is presently directed to the cathode side of the cells. The cathode material must be stable, porous, and conducting, a good catalyst for the oxygen reduction, and compatible with zirconia in terms of thermal expansion. A group of perovskite-type oxides are promising candidates. In 1989, the formation, stability, and electrical properties of some of these, e.g. $La_{0.8}Sr_{0.2}MnO_3$ ("LSMO") and $La_{0.8}Ca_{0.2}MnO_3$ ("LCMO"), were studied. The following are examples of studies of the chemistry and electrochemistry of the interface between such cathode materials and zirconia.

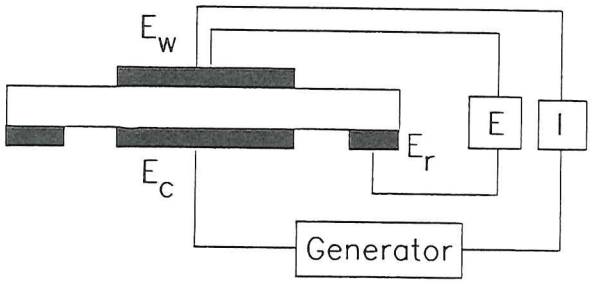

Fig. 2. Schematical cross section of solid electrolyte tablet (white) with LCMO electrodes (black).

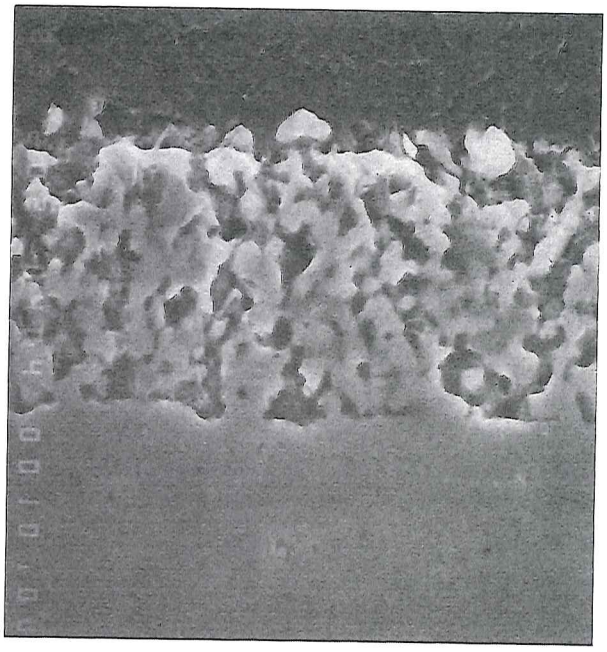

Fig. 3. SEM micrograph of cross section of YSZ–LCMO interface.

Characterization of an LCMO – zirconia electrode interface

Polymer-based slurries of LCMO were painted onto sintered, dense YSZ tablets and burned at 1200 °C for 12 hours to form porous electrodes, as shown in Figs. 2 and 3. The two centered electrodes served as working electrode (E_w) and counter electrode (E_c). A third electrode was painted as a circle close to the edge of the sample and served as reference electrode (E_r).

By supplying a current I through E_w and E_c and measuring the voltage E between E_w and E_r, the current–voltage-characteristics of the working electrode can be established, without contributions from the other two electrodes. The voltage developed in the electrolyte between E_w and E_r (IR-drop) will contribute, but can be ruled out by various methods.

In Impedance Spectroscopy (IS), an alternating current (AC) is applied, and, through the measured voltage, the AC-impedance of E_w is obtained (10^{-5} to 10^7 Hz). Figure 4 shows an impedance spectrum (imaginary vs real impedance) for the working electrode taken at 900 °C in air. Characteristic frequency dependencies of the real and imaginary impedance of different electrochemical processes or sample microstructures enable a deconvolution of the spectrum. In broad terms, the diameter of the semicircle along the real axis can be attributed to the charge transfer resistance (R_{ct}) of the reaction $O_{ads.} + 2e^- = O^{2-}$. The distance from origo to the left part of the semicircle is attributed

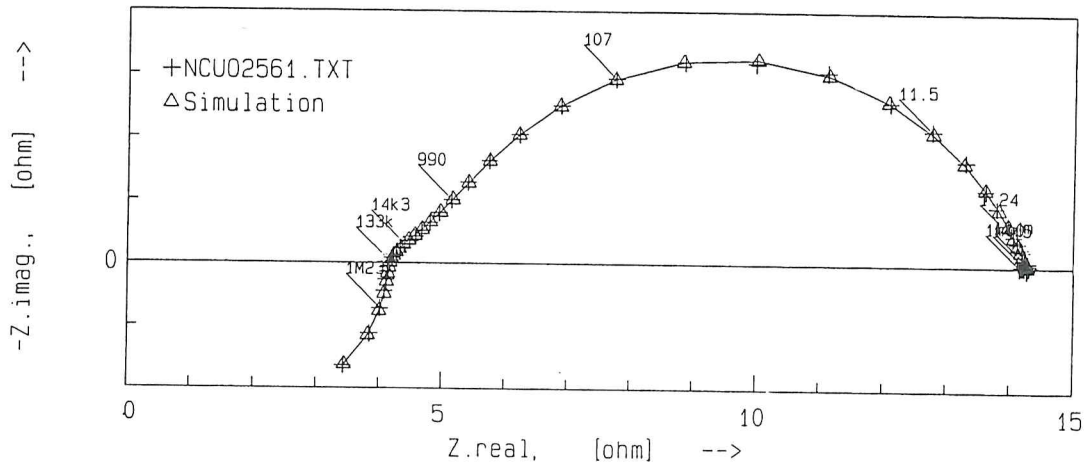

Fig. 4. Complex plane impedance plot showing fit between the measured spectrum and an equivalent circuit model spectrum. Numbers along the curve represent measurement frequency.

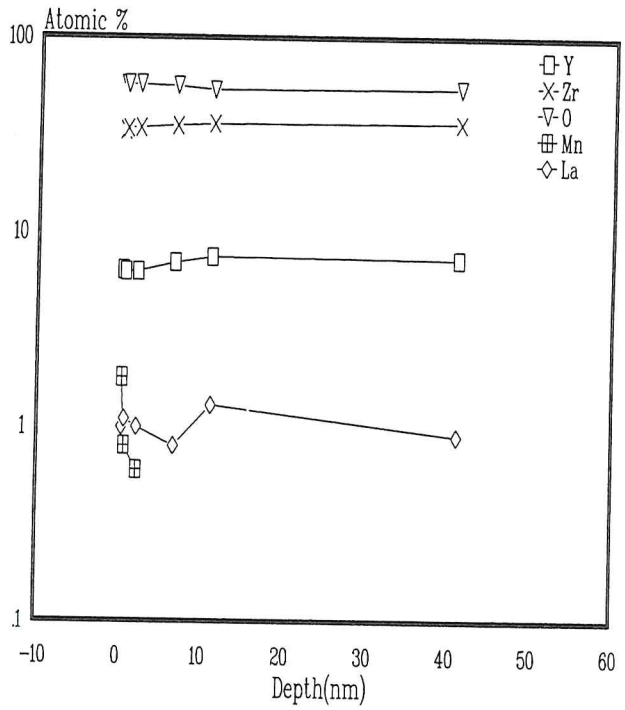

Fig. 5. XPS depth profile, from the original LCMO–YSZ interface, into the YSZ.

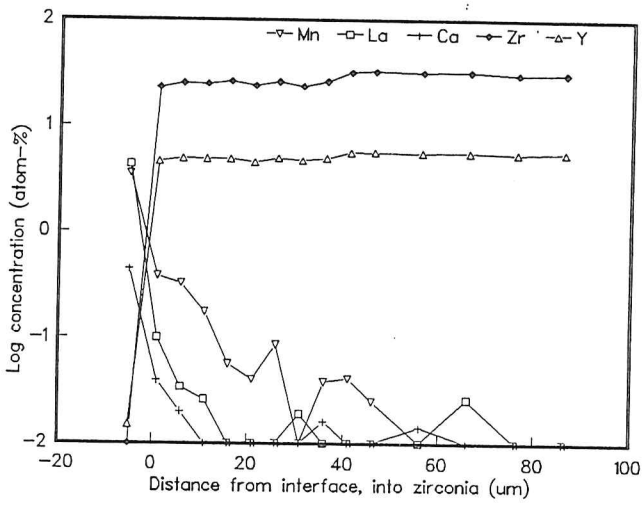

Fig. 6. Electron microscopy analysis over cross section of LCMO–YSZ interface. Negative distance is into the LCMO, positive distance is into the YSZ.

to the IR-drop. An R_{ct} of around 10 ohms would cause unacceptably high cathodic overpotential losses in an SOFC. Minimizing R_{ct} is one of the ultimate goals of the research.

It is important to correlate the electrode resistance with electrode porosity and grain size, since these factors determine the number of zirconia–LCMO–gas three-phase reaction sites.

In order to study interdiffusion and reaction between LCMO and zirconia, the LCMO was removed mechanically from the zirconia, and rests of LCMO were etched away with HCl. The exposed zirconia surface was analyzed with XPS, and argon ion sputtering down to around 100 nm yielded a depth profile, as shown in Fig. 5. It appears that Mn and La from the LCMO is only present in 1–2 atom-% in the surface of the zirconia, and a reaction product phase is thus not observed. Diffusion of Mn and La into the zirconia is relatively slow, and the levels drop to below the detection limit (around 0.3 atom-%) within a few nanometers from the interface in the case of Mn, and a few tens of nanometers in the case of La.

Furthermore, a cross-section of the interface was analyzed in a SEM. The analysis vs. distance from the LCMO–zirconia interface is shown in Fig. 6. This method works on a lateral length scale orders of magnitude coarser than in XPS depth profiling, revealing that small levels of Mn and La diffused several micrometers into the zirconia. In all probability, this reflects grain boundary diffusion, while the XPS depth profile reflects bulk diffusion. In Fig. 6 it may be noted that neither Zr nor Y seem to diffuse very fast into the LCMO.

Truls Norby

Abstracts

of Publications and Proceedings printed or submitted during 1989

Andersen, A. G. and Norby, T.
"Liquid phases in Li:MgO as studied by thermoanalytical methods, electron microscopy, and electrical conductivity measurements."
Proceedings of the Second European Workshop on Catalytic Methane Activation, Enschede, The Netherlands, 1989.

The phase relations in parts of the system Mg–Li–O–H–C are reviewed and some features investigated by TG, DTG, DSC, SEM, TEM, and electrical conductivity measurements on a commercial Li:MgO catalyst. Electrical conductivity measurements on samples with varying Li contents are used to monitor the presence of highly conducting surface melts under controlled atmospheres at high temperatures. The measurements indicate that the solubility of lithium in MgO bulk increases with increasing oxygen activity, as predicted by defect theory. The solubility of Li in MgO at 700 °C in CO_2-rich, oxidizing atmosphere is estimated to be of the order of magnitude of 0.1 mol-% (0.02 wt-%).

Andresen, A. F., Bärner, K., Fjellvåg, H., Kjekshus, A., Rager, H., Sondermann, U. and Stølen, S.
"Influence of Phosphorus Substitution on $Mn_{0.63}Cr_{0.37}As$."
J. Magn. Magn. Mat. submitted.

$Mn_{0.63}Cr_{0.37}As_{1-x}P_x$ has been investigated for $0.00 \leq x \leq 0.10$ by X-ray and neutron diffraction, magnetometric, DTA, DSC and ESR measurements. The results show that there is complete solid solubility throughout the studied composition range with random distribution of Mn, Cr ans As, P over the metal and non-metal sublattice, respectively. At and below room temperature the crystal structure is of the MnP type. Phosphorus acts as a positive chemical pressure generator. The characteristic magnetic transitions of $Mn_{0.63}Cr_{0.37}As$ on decreasing temperature, para (P) to helimagnetic (Hc) followed by Hc to Ha, are only maintained at a very low substitution level, $x < 0.008$. Further increase of the phosphorus content surpresses Hc and favours ferromagnetism (F). For $x > 0.05$ the F mode becomes the only ordered magnetic state. A tentative magnetic phase diagram for $Mn_{0.63}Cr_{0.37}As_{1-x}P_x$ ($0.00 < x < 0.10$) is advanced. Interesting features of ESR data are presented, and connections to the magnetic phase diagram are proposed.

Becerra, C. C., Zieba, A., Oliveira, N. F. Jr. and Fjellvåg, H.
"Magnetic Phase Diagram of $Mn_{0.9}Co_{0.1}P$ Single Crystal. Irreversibility Behaviour in a Magnetic Field."
Proc. of 34th Annual Conf. on Magnetism and Magnetic Materials, Boston, USA, November 1989; J. Appl. Phys. **67** (1990) 5442–45.

The magnetic phase diagram of a $Mn_{0.9}Co_{0.1}P$ single crystal was studied by AC susceptibility with a magnetic field (H) applied along its orthorhombic b axis. This system orders ferromagnetically at 197.5 K and below 37 K it shows a helimagnetic structure in H = 0. The H–T phase diagram above 37 K is similar to the one found in pure MnP. Including the presence of a Lifshitz multicritical point (H_L = 11.0 kOe, T_L = 99 ± 1 K) at the confluence of the paramagnetic, ferromagnetic and modulated fan-like phase. It was found that: (1) the hysteresis at the first-order transitions between the ordered phases is much larger than in MnP; (2) hysteretic behaviour is observed inside the whole

region of the phase diagram corresponding to the fan-like phase; (3) the second-order fan – para transition fades at low temperatures and an irreversible behaviour is observed with the irreversibility field sharply increasing at lower temperatures. The last feature is in marked contrast with what is observed in pure MnP, where the second-order fan – para transition is very sharp and the transition field tends to constant value at low temperatures.

Bergsmark E., Simensen, C. J. and Kofstad, P.
"The Oxidation of Molten Aluminium"
Mater. Sci. Eng. **A120** (1989) 91–95.

Oxidation of molten aluminium of commercial purity (Mg–50 ppm; Li–4 ppm; Na–2 ppm and Ca–2 ppm) in oxygen at different partial pressures has been studied at 800–950 °C. Reaction rates and kinetics have been measured by thermogravimetry and reaction products have been characterized by X-ray diffraction, scanning electron microscopy and electron microprobe analyses.

The reaction kinetics are complex and can not be described by simple rate equations. Plots of weight gain versus time have an approximate S-shaped form. The oxide scales formed after extended reaction consist of i) a thin, relatively compact layer of aluminium oxide next to the metal, ii) on top of this a thicker and porous layer of aluminium oxide with inclusions of unreacted aluminium particles, and iii) oxide outgrowths on the oxide surface, some of which consist of magnesium oxide.

The rates of oxide growth are faster than values calculated from reported lattice self-diffusion coefficients of oxygen and aluminium by more than seven orders of magnitude. It is concluded that growth of the compact oxide takes place by diffusion along easy diffusion paths. Cracking of the scales also contributes to yield complex kinetics. An additional feature is that magnesium is transported rapidly through the scale and forms the MgO-rich part of the outer surface.

Dugstad, A. and Videm, K.
"CO_2-Corrosion of Steel Drums for Active Waste at Low Temperature and Low CO_2 Partial Pressure."
Proceedings 11th Scandinavian Corrosion Congress, Stavanger 1989, paper F–46.

The experiments were carried out in order to generate data for prediction of corrosion rates of waste containers of steel in a water containing carbon dioxide due to microbiologic decomposition of celluloce. The corrosion rate will be limited by the rate of carbon dioxide production as this constituent is consumed by the corrosive reactions. However, also iron oxides or hydroxides can be formed together with ferrous carbonate, but at a rate which leads to a rather small increase in the corrosion rate.

Dugstad, A. and Videm, K.
"Radioactive Techniques for Corrosion Monitoring."
NACE Corrosion/89 1989, p. 47.

In-situ corrosion rate measurements by utilizing induced radioactivity in the metal has been found very cost efficient. The corrosion rate has been monitored continously by radiation counters placed at a convenient location outside the test equipment, taking advantage of the abilitlity of gamma rays to penetrate metals. The corrosion rate is determined by the loss of radioactivity due to the removal of radioactive metal by the corrosive reactions. The measurements are fully non-destructive, easy to interprete and accurate. The normal sensitivity is 0.1% of the thickness of the radioactive metal, e.g. with a 1 mm thick coupon corroded from both sides 0.5 micron metal loss is detectable. The report also briefly describes other uses of radioactivity in corrosion research.

Dugstad, A. and Videm, K.
"Radioactive Tecniques for Corrosion Monitoring."

11th European Corrosion Congress, Utrecht, 1989, p. 47.

(Shortened verson of paper above.)

Fjellvåg, H., Karen, P., Kjekshus, A. and Andresen, A. F.
"Superconducting Properties in Relation to Chemical Pressure in $YBa_2Cu_3O_{9-\delta}$."
Proc. Conf. Materials and Mechanisms of Superconductivity, High Temperature Superconductors, II, Standford, California USA, July 1989; Physica C. **162–164** (1989) 49–50.

Based on oxygen analysis and investigations by X-ray and neutron diffraction of single phase samples, structural consequenses of substitution of La or Sr for Ba in $YBa_2Cu_3O_{9-\delta}$ are rationalized in terms of a chemical pressure concept. Due to the size imbalance, a strain is introduced into the $[Cu_3O_{9-\delta}]n$ network upon substitution. The resulting contraction is rather isotropic in case of Sr, while upon the La substitution, the c-axis is contracted preferably. As a result of this anisotropy, the orthorhombic distortion of the structure diminishes (vanishes at 16% La substitution for $9-\delta = 6.97$), being accompanied by redistribution of oxygens towards giving octahedral coordination for Cu. A decrease in the distortion is observed when the oxygen content itself is varied from $9-\delta = 6.97$ in both directions. T_c decreases both with La (4.6 K/%) and Sr (0.3 K/%) substitutions. Independent of the actual degree of the orthorhombic distortion, T_c increases with increasing oxygen content if the additional oxygens are brought by La. At a constant oxygen content, T_c is coupled to the Jahn–Teller distortion of the Cu-coordination octahedra, and thus approximately related to the ratio of the (orthorhombic) unit cell dimensions; $D_{JT} = 100\ [\ 2c/3(a+b) - 1]\ (\%)$. Possible analogies to other systems are discussed.

Fjellvåg, H., Kjekshus, A., Zach, R. and Zieba, A.
"$Mn_{1-t}(Ti_{0.50}V_{0.50})_tAs$; Diluted Manganese Arsenide with Zero Overall Chemical Pressure."
J. Phys. Chem. Solids **50** (1989) 187–195.

The $Mn_{1-t}(Ti_{0.50}V_{0.50})_tAs$ solid solution phase has been studied by means of powder X-ray diffraction, DTA measurements, and various magnetometric methods including application of pressures up to 10 kbar. $Mn_{1-t}(Ti_{0.50}V_{0.50})_tAs$ provides a purposely produced example of an essentially zero overall chemical pressure phase (the volume stays constant within ±0.3% at 450 K) with marked anisotropy features. The magnetic phase diagram shows a first order MnP,P– to NiAs,F-type transition for $0.00 \leq t \leq 0.20$ and a continuous NiAs,P NiAs,F-type transition from $t = 0.20$ up to the stability limit of the ferromagnetic mode at $t = 0.70$. The applicability of the classical model for magneto-elastic coupling (modified to include the effects of dilution and anisotropy) to $Mn_{1-t}(Ti_{0.50}V_{0.50})_tAs$ and related cases is discussed.

Fjellvåg, H., Lillerud, K. P., Norby, P. and Sørby, K.
"Structural Properties of some Ferrierite-Type Zeolites."
Zeolites **9** (1989) 152–158.

The zoelite ferrierite was synthesized from a sodium and tetramethylammonium (TMA) containing gel. Powder X-ray diffraction data show the basic framework for natural and synthetic ferrierite to be similar. X-ray diagrams of natural ferrierite are frequently burderened by effects from preferred orientation of the crystallites. The (110) reflection is generally of much less intensity than expected from pattern simulation based om published crystal structure data. The temperature-induced changes in the unit cell dimensions of synthetic ferrierite (with TMA as template, in the calcined form, and in the H-

form) are presented, and the contraction of the unit cell correlated with weight losses as determined thermogravimetrically. The thermally induced changes in the framework of H-ferrierite are discussed.

Fjellvåg, H., Nørlund Christensen, A. and Pannetier, J.
"$SbTaO_4$ – Formation and Thermal Properties."
Acta Chem. Scand. submitted.

The solid state reaction between Sb_2O_3 and Ta_2O_5 with formation of $SbTaO_4$ has been studied by means of time resolved powder neutron diffraction. High-temperature powder diffraction studies show, contary to earlier reports, that no discontinuous phase transitions occur for $SbTaO_4$, or for the $Sb_{1.2}Ta_{0.8}O_4$ solid solution phase at temperatures between 300 and 1300 K. For $Sb_{1.2}Ta_{0.8}O_4$ small changes in the temperature dependence of the unit cell dimensions around 800 K, may reflect the ferro– to paraelectric phase transition.

Fjellvåg, H., Stølen, S., Grosshans, W. A. and Krüger, T.
"Equation of State of $MnAs_{0.88}P_{0.12}$."
J. Solid State Chem. **87** (1990) 222–228.

The influences of external pressures, up to 30 GPa, on the structural properties of $MnAs_{0.88}P_{0.12}$ has been studied for temperatures between 300 and 450 K by energy dispersive X-ray diffraction using synchrotron radiation. $MnAs_{0.88}P_{0.12}$ undergoes a very large, continuous volume contraction when subjected to pressure. The experimental pV–relationship is discussed on the bais of the first order Birch and Murnaghan equations of state, and the structural changes are discussed in relation to similar observations for isostructural (MnP type) phases. The experimental results at 300, 350 and 450 K are in excellent agreement with earlier estimations of the temperature dependence of the compressibility which were based on the chemixal pressure concept with starting point in the equivalency of the p,T– phase diagram of MnAs and the x,T– phase diagram of $MnAs_{1-x}P_x$. The isothermal bulk modulus B_o and its pressure derivative B_o' are according to the Murnaghan equation of state respectively 18 GPa and 10 at 300 and 450 K, and respectively 10 GPa and 18 at 350 K. Values for the Gibbs energy and the entropy at 300 K are tabulated as function of pressure.

Gonzales–Alvarez, D., Grønvold, F., Falk, B., Westrum Jr. E. F., Blachnik, R. and Kudermann, G.
"FeAs: Heat capacity, enthalpy increments and other thermodynamic properties from 5 to 1350 K, and magnetic transition."
J. Chem. Thermodynamics **21** (1989) 363–373.

The heat capacity of iron monoarsenide has been determined by adiabatic calorimetry from 5 to 1030 K and by drop calorimetry relative to 298.15 K over the range 875 to 1350 K. A small λ-type transition is observed at T_N = (70.95 ±0.02) K. It is related to the disappearance of a doubly helically ordered magnetic-spin structure on heating. The obviously cooperative entropy increment of transition is only $\Delta_{trs}S_m/R$ = 0.021. The higher-temperature heat capacity rises considerably above lattice expectations. Part of the rise is ascribed to low-spin electron redistribution in iron, while the further excess above 800 K presumably arises from a beginning low– to high-spin transition, possibly connected with interstitial defect formation in the MnP-type structure. FeAs melts at about 1350 K with $\Delta_{fus}H_m$ = 6180R K. Thermodynamic functions have been evaluated and the values of $C_{p,m}(T)$, $S_m(T)$, $H_m(T)$, and $\Phi_m(T)$, are 6.057*R*, 7.513*R*, 1177*R*·K, and 3.567*R* at 298.15 K, and 8.75*R*, 16.03*R*, 6287*R*·K, and 9.745*R* at 1000 K.

Gulbrandsen, E.
"Pitting Corrosion of Magnesium in Sulphate Containing Alkaline Solutions."
Proc. 11th Scandinavian Corrosion Congress, Stavanger 1989, paper F–39.

The title subject has been studied with high purity (99.98%) magnesium electrodes in deoxygenated unbuffrered, phosphate buffered and $Mg(OH)_2$ saturated solutions (pH 7.1–13) with additions of 10^{-4} to 1 M sulphate. Potentiostatically measured critical potentials for pit nucleation (Enp) are reported and briefly discussed with respect to several existing pit nucleation theories. Enp appears to be a function of the sulphate concentration, the pH, the phosphate buffer concentration, the metal purity and the stabilization time at potentials below Enp. No simple quantitative relations have been found, however. The pits always appear to be hemispherical, and the corrosion attack appears less severe in sulphate than in corresponding chloride solutions.

Häggstrøm, L., Gustavson–Seidel, A. and Fjellvåg, H.
"A Mössbauer Study of Helimagnetic FeAs."
Europhys. Lett. **9** (1989) 87–92.

The ^{57}Fe Mössbauer spectra of FeAs above the Néel temperature, 77 K, display an electric-quadropole split doublet with a splitting of 0.55 mm/s at 295 K. This value increases almost linearly (0.05 mm/s per 100 K) with decreasing temperature, a change which can be correlated to the decreasing Fe–As nearest neighbour distance. Below 77 K a complex, partly nonresolved Mössbauer pattern develops. The magnetic hyperfine field varies strongly with the rotation of the magnetic moment in the (a, b) plane, giving values between 4.8 T and 1.6 T. Using the conversion factor 10 T/m_B the average magnetic moment would be 0.30 m_B. Whether these highly anisotropic hyperfine fields also correspond to an anisotropic distribution of magnetic moments is still an open question.

Holt, A. and Kofstad, P.
"High temperature corrosion of iron in O_2 + 4% SO_2/SO_3 at 500–800 °C."
Mater. Sci. Eng. **A120** (1989) 101–104.

The reaction of high purity iron with a gas mixture of O_2 + 4% SO_2/SO_3 has been studied in the temperature range 500–800 °C. Reaction kinetics were followed by thermogravimetry and reacted specimens were characterized by X-ray-diffraction, X-ray photoelectron spectroscopy and scanning electron microscopy.

The reaction rate increases with increasing temperature at 500–640 °C, but around 640 °C the rate constant drops by about an order of magnitude for then again to increase with increasing temperature. The rapid reaction rate at lower temperatures takes place under conditions when iron(III)sulphate is formed on the surface. The inner layer of the scale then consist of Fe_2O_3, Fe_3O_4, $Fe_{1-y}O$ (depending on the temperature) and $Fe_{(1-x)}S$. It is suggested that the sulphide phase is distributed as a three-dimensional network in the inner layer of the scale and serves as a path for rapid outward diffusion of iron and thereby the rapid reaction rate. At higher temperature the scale has the same composition as for oxidation of iron in oxygen and consist of Fe_2O_3, Fe_3O_4 and $Fe_{1-y}O$. In addition small amounts of $Fe_{(1-x)}S$ are detected at the metal/scale interface. This sulphide is probably formed during the initial reaction of iron with the gas mixture.

Hönle, W., Furuseth, S. and von Schnering, H. G.
"Synthesis and Crystal Structure of Ordered, Orthorhombic α–$NbBr_5$."
Z. Naturforsch. **45b** (1990) 952–956.

Niobium pentabromide, $NbBr_5$, is prepared in the orthorhombic ordered (α)-form from the elements in sealed quartz ampoules (Nb powder, Br_2, *l*) at 973 K. The structure has been determined from single crystal data (a = 1288.8(2) pm, b = 1869.0(3) pm, c = 614.9(1)

pm; Pnma (no. 62); Z = 8; R = 0.055). α-$NbBr_5$ forms dimeric Nb_2Br_{10} molecules with d(Nb–Br_b) = 271.5 pm, d(Nb–Br_e) = 240.8 pm and d(Nb–Br_a) = 246.1 pm. α-$NbBr_5$ is a diamagnetic semiconductor with ${}^{cgs}X_{mol}$ (300 K) = $-72 \cdot 10^{-6}$ cm^3/mole. The band gaps of $NbCl_5$, α-$NbBr_5$ and NbI_5 have been determined by diffuse reflection to be $E_g(NbCl_5)$ = 2.74 eV, E_g(α-$NbBr_5$) = 1.99 eV, and $E_g(NbI_5)$ = 0.99 eV.

Hornkjøl, S.
"Kinetics of Pitting Corrosion on Zirconium in Mixed Chloride–Sulphate Solutions."
Acta Chem. Scand. **43** (1989) 647–650.

Pitting initiation on zirconium in chloride-containing sulphate solutions has been studied and a possible model for the reaction mechanisms has been developed. The model is based on considerations concerning the localized adsorption of the two anions. It agrees with the experimental results in showing second-order stimulation of the pitting initiation by chloride ions and first-order inhibition by sulphate ions.

Hornkjøl, S.
"Effects of Oxalate Ions on the Corrosion of Niobium."
Acta Chem. Scand. in press.

At pH below 4, oxalate ions/oxalic acid is found to increase the corrosion of niobium. The corrosion current is half-order dependent of the concentration of oxalate ions/oxalic acid in the solution.

Hornkjøl, S. and Hurlen, T.
"Anodic Growth of Passive Films on Zirconium and Hafnium."
Electrochim. Acta. Submitted Aug. 1989.

Galvanostatic potential–time curves on passive zirconium and hafnium electrodes are recorded and analyzed in the light of the Cabrera–Mott equation and the high-field ion migration equation. For both metals, the kink-site density in the reacting metal surface appears to attain a steady value which depends on the current density of metal oxidation according to d log s/d log j = 0.5. This is supported by polarization data from potentiostatic transients on a time scale of seconds. Possible effects of space charge in the passive film are considered and found to be negligible under the conditions covered. Comparisons are made with behaviour of some other passive metals and with the anodic dissolution of some active metals.

Hornkjøl, S. and Wilhelmsen, W.
"Electron Transfer Reactions of the Hexacyanoferrate Redox Couple at Passive Niobium."
Acta Chem. Scand. in press.

The electron transfer reactions of the hexacyanoferrate redox couple on passive niobium has been studied and reaction orders have been determined at different pH. The solution chemistry appears to explain the fractional reaction orders found. Anodic oxidation is very slow and the exchange current density is extremely low. Comparisons have been made with measurements on other metals, especially Ti.

Hurlen, T., Simon, C., Wilhelmsen, W., Hornkjøl, S. and Gulbrandsen, E.
"Model Studies on Passive Metal Electrodes."
Electrochim. Acta **34** (1989) 519–524.

Studies are made on passive metal electrodes with n-type semiconducting (or insulating) passive films. Emphasis is on conditions in which such films are electronically exhausted, but not inverted. Considerations are especially made of defect production and transport in passivating oxide films and of acid-base equilibria at oxide/solution interfaces. Expectations are derived for the donor, charge and Volta potential profiles of passive

metal electrodes and, hence, for their electrode potential and capacitance behaviour and for their band structure. Comparisons are made to observations on aluminium, iron, titanium, zirconium, hafnium, niobium and tantalum. Of these metals, however, only Al, Nb and Ta exhibit the capacitance behaviour expected. It appears that field-dependent surface potentials (dipole layers) should be invoked, and that adsorption of other ions than protons and hydroxide ions should also be considered.

Khanna, A.S. and Kofstad, P.
"Effect of Temperature, Pressure and Flow Rate on the Oxidation of 304 Stainless Steel in Dry and Wet Oxygen."
Metals Materials and Processes **1** (1989) 177–196.

Oxidation studies have been carried out on 304 stainless steel in dry oxygen and in oxygen containing 2% water vapour. While a thin compact layer of chromium oxide was formed in the dry oxygen, the scale formed in wet gas was porous and consisted mainly of iron rich oxide. The oxidation behaviour is found to be influenced by several factors. Results showing the effect of temperature, flow rate and pressure on the oxidation rate are presented. Short and long terms experiments have been carried out using thermogravimetry and the results have been substantiated by careful analyses of scale of various stages of oxidation. The most important effect of water vapour is to increase the rate of diffusion. This results in faster depletion of chromium in the underlying matrix causing the diffusion of iron and thus in the formation of iron rich scales.

Kofstad, P.
"Aspects of High Temperature Corrosion of Metals by Gases in Thermochemistry of Alloys."
Ed. Brodowsky, H. and Schaller, H.–J. Kluwer, Academic Publishers, Dordrecht, Nederland, 1989, p. 471–480.

The paper surveys high temperature corrosion phenomena involving diffusion-controlled growth of continuous scales. Lattice diffusion is rate-determining only for scales with relatively high concentrations of point defects and at high temperatures, e.g. oxidation of Co to CoO above about 1000 °C. At more reduced temperatures and for scales with relatively low defect concentrations scale growth predominantly takes place by grain boundary diffusion, e.g. growth of NiO, Cr_2O_3, and Al_2O_3. The common use metals may corrode rapidly in many sulfur-containing atmospheres due to the formation of sulfide phases which are highly nonstoichiometric and exhibit high rates of diffusion. This is illustrated for corrosion of metals and dilute nickel alloys in O_2 + SO_2/SO_3 atmospheres. It is emphasized that the distribution of the sulfide phases in the scales is important for the reaction mechanism.

Kofstad, P.
"Appraisal Keynote: Future Trends and Developments, in The Role of Active Elements in the Oxidation Behaviour of High Temperature Metals and Alloys."
Ed. Lang, E., Elsevier Applied Science, London/New York, p. 367–370.

The paper briefly summarizes important effects of active elements on the oxidation behaviour of metals and alloys – particularly using chromia scales as examples. In the author´s evaluation available results suggest that the effects may generally be interpreted on the basis of the following mechanistic model: i) scale growth mainly takes place through grain boundary diffusion and ii) the active elements exert their effects through enrichment/segregation at grain boundaries and thereby on the diffusional transport through the scales, grain growth, high temperature creep, etc. of the scales.

With regard to future trends and development the author is convinced that the key to

understanding effects of active elements – and also many other aspects of protective oxidation – lies in improved understanding of interfaces and grain boundaries (structures, enrichment/segregation phenomena, transport properties) and the resultant effects on growth and properties of protective scales. Such knowledge can only be obtained through the characterization coupled with carefully controlled reaction studies. It is proposed that a coordinated, cooperative research programme should be initiated in order to secure faster progress in the field and to obtain necessary data for developing high temperature materials.

Kofstad, P.
"Fundamental Aspects of Corrosion by Hot Gases."
Mater. Sci. Eng. **A120** (1989) 25–29.

The fundamental importance of external surfaces, interfaces and grain boundaries is emphasized by a few selected examples of corrosion of metals by hot gases. In the author´s opinion, fundamental knowledge of their structures and "defect structures", enrichment – segregation phenomena, transport properties, etc. provides a key to many questions that still face us in the field high-temperature corrosion.

Kofstad, P., Rahmel, A., Rapp, R. A. and Douglass, D. L.
"International Workshop on New Fundamentals of Scale Growth."
Oxidation of Metals **32** (1989) 125–166 (no abstract).

Koksbang, R., Fauteux, D., Norby, P. and Nielsen, K. A.
"Lithium Insertion in $LiCr_3O_8$, $NaCr_3O_8$ and KCr_3O_8 at Room Temperature and at 125 °C."
J. Electrochem. Soc. **136** (1989) 598–605.

Lithium insertion and deinsertion reactions have been carried out with $LiCr_3O_8$, $NaCr_3O_8$ and KCr_3O_8 chemically and electrochemically at room temperature and at 125 °C. The electrochemical experiments were performed with a nonaqueous liquid electrolyte at room temperature and with a polymer electrolyte at high temperature. At both temperatures, $LiCr_3O_8$ inserts chemically and electrochemically ca. 4 and 5 Li per formula unit, respectively. Experimental data reveal that the reaction involves major structural changes. At elevated temperatures, the isostructural compounds $NaCr_3O_8$ and KCr_3O_8 are able to accommodate more than 4 Li/MCr_3O_8. During this process, minor structural changes are observed. At room temperature, $NaCr_3O_8$ and KCr_3O_8 also accommodate Li topotactically, but the maximum number of Li inserted per formula unit is close to 4 Li/$NaCr_3O_8$ and 1.3 Li/KCr_3O_8. Lithium ion diffusion coefficients are similar for the two compounds in the comparable composition range. Thermally, the fully lithiated compounds appear to be as stable as the pristine materials.

Krogh Andersen, I. G., Krogh Andersen, E., Norby, P., Colella, C. and de´Gennaro, M.
"Synthesis and Structure of an ABW Type Thallium Aluminosilicate."
Zeolites, in press.

Tl–ABW, $TlAlSiO_4$ was prepared hydrothemally in presence of Li^+, Na^+ and K^+ ions and its structure was determined from X-ray powder diffraction data. The unit cell is a = 8.297(1), b = 9.417(1), c = 5.413(1) Å, and the space group is $Pna2_1$, No 33, Z = 4. The structure was refined using powder diffraction data by the Rietveld profile refinement technique. The anion framework has an ordered Si/Al distribution. The extra framework cations (Tl^+) occupy three partially populated positions. The structure is described and the synthesis of Tl–ABW in presence of lithium, sodium and potassium ions is discussed.

Norby, P.
"Thermal Transformation of Zeolite Li–A(BW): The Crystal Structure of γ-Eucryptite, a Polymorph of $LiAlSiO_4$."
Zeolites **10** (1990) 193–199.

Among the thermal transformation products of zeolite Li–A(BW), $LiAlSiO_4 \cdot H_2O$, a number of polymorphs with composition $LiAlSiO_4$ are observed. The transformation does not involve formation of intermediate amorphous phases. Reversible dehydration of the zeolite is possible to a limited extent; thereafter, the structure collapses into an anhydrous phase. Rehydration to zeolite Li–A(BW) is only possible using prolonged hydrothermal treatment. A structural model for the anhydrous phase related to the ABW type is proposed. At 650 °C γ-eucryptite is formed, and its structure is monoclinic with a = 8.228(2), b = 5.032(1), c =8.274(1) Å, and β = 107.46(1)°, spacegroup Pa. Its crystal structure was determined and refined using combined information from MAS n.m.r. spectroscopy and X-ray and neutron powder diffraction. γ-eucryptite has a stuffed cristobalite-type structure with the lithium ions having distorted tetrahedral coordination. A mechanism for the transformation from the ABW type structure to the cristobalite type is proposed. At 900–1000 °C γ-eucryptite transforms into the final high-temperature polymorph β-eucryptite.

Norby, P., Krogh Andersen, I. G., Krogh Andersen, E., Colella, C. and de´Gennaro, M.
"Synthesis and Structure of Lithium Cesium and Lithium Thallium Cancrinites."
Zeolites, in press.

X-ray powder diffraction studies of synthetic cancrinites were undertaken to elucidate the role of lithium ions and large cations (Cs, Tl) in zeolite crystallizations. $Li_{4.56}Cs_{1.50}Al_6Si_6O_{24} \cdot 4.9H_2O$ has a = b = 12.4328(12), c = 4.9692(6) Å, $P6_3$, Z = 1. The structure was refined by Rietveld profile refinement technique. The cesium ions located in the cancrinite cage only, are coordinated to twelve oxygen atoms (at distances 3.14 to 3.61 Å). In accordance with their positions they are not exchangeable. The lithium ions are four coordinated to oxygen atoms (at distances 1.91 to 2.03 Å). $Li_{2.75}Tl_{3.23}Al_{5.85}Si_{6.13}O_{24} \cdot 2H_2O$ has a = b = 12.4419(7), c = 4.9884(4) Å, $P6_3$, Z = 1. The thallium ions are located on more than one posistion in the cancrinite cage, and there is also thallium on one position in the channels. This is in accordance with the thallium ions being partially exchangeable in this material. The structures are described and the action of small and large cations in cancrinite crystallization is discussed.

Norby, T.
"Hydrogen Defects in Inorganic Solids."
Studies in Inorganic Chemistry, 9; "Selected topics in high temperature chemistry; Defect Chemistry of Solids" (Andersen, A. G. og Johannesen, Ø., eds.), Elsevier, Amsterdam, 1989.

The defect chemistry and transport of hydrogen in ceramics, as well as relevant experimental methods, are reviewed, with examples from the literature. The treatment concentrates on behaviour of protons in oxides at high temperatures, but often in view of the more established low-temperature chemistry of protons. Other classes of compounds and other hydrogen species are discussed more briefly.

Norby, T.
"Protons in ZrO_2; A search for effects of water vapour on the electrical conductivity and M/T phase transformation of undoped ZrO_2."
In "Zirconia 88", Elsevier, Amsterdam, 1989.

The transformation temperatures and rates of the M–T and T–M phase transformations of undoped ZrO_2 have been studied at high tem-

peratures as a function of the water vapour pressure in oxygen or air. The transformation was studied by recording the electrical conductivity of a sintered, porous sample with Pt-foil electrodes. No effect of the water vapour pressure could be detected. However, the conductivity of monoclinic zirconia was dependent on the water vapour pressure. The conductivity of the tetragonal phase, on the other hand, did not depend on the water vapour pressure. It is concluded that protons are significant defects in monoclinic zirconia, while they are minority defects in tetragonal zirconia.

Norby, T.
"Proton Conduction in Oxides."
Proceedings of the 7th International Symposium on Solid State Ionics, to appear in Solid State Ionics.

The nature of proton defects in oxides is described briefly. Literature data for the concentration, diffusivity, and conductivity of protons in oxides are reviewed and discussed.

Sharkawy, B., Abu–Zahara, Hammad, H. H. and Videm, K.
"Influence of some factors on the susceptibility of Zircaloy tubes to iodine stress corrosion cracking."
Journal of Nuclear Materials **165** Nr 2. (1989).

Shaviv, R., Westrum Jr., E. F., Grønvold, F., Stølen, S., Inaba, A., Fujii, H. and Chihara, H.
"Heat capacity, thermodynamic properties and transitions of silver iodide."
J. Chem. Thermodynamics **21** (1989) 631–651.

The heat capacity of silver iodide was measured using adiabatic calorimetric cryostats over the ranges 7 to 350 K and from 2 to 75 K. The (β to α)- and (β/γ to α)-transitions and the heat capacities of single crystals of β-, of finely divided β/γ-, and of the α-phases were measured in adiabatic calorimetric cryostats and thermostats from 70 to 700 K and from 310 to 523 K. The values of $C_{p,m}$, S_m, and Φ_m at 298.15 K are 6.707 R, 13.764 R, and 8.511 R for the β-phase and since the molar volumes of β- and γ-phases are identical and the structures differ only in their stacking sequence, their heat capacities are essential identical. Moreover, the molar transition-enthalpy increments to the α-phase of the two samples are also equal within the accuracy of the present measurements in spite of the structural differences occasioned by the precence of some γ-AgI in one of them (below the transition temperature). The (partial) enthalpy of the (β/γ to α)-phase transition was found to be (758.7 ±0.8)R·K and that of the(β to α)-phase transition was found to be (758.0 ±0.3)R·K over the range 405 to 425 K mean:(758.4 ±0.4)R·K. The (total) enthalpy of transition is about 1150R · K. An abnormal trend in the heat capacity values are compared with those of prior overlapping measurements by Nernst and Schwers, by Pitzer, and by Madison *et al.* for the β/γ-phase, and in and beyond the transition region with those of numerous prior investigators.

Shaviv, R., Westrum Jr., E. F., Fjellvåg, H. and Kjekshus, A.
"$ZrTe_5$ and $HfTe_5$: The Heat Capacity and Derived Thermophysical Properties from 6 to 350 K."
J. Solid State Chem. **81** (1989) 103–111.

The heat capacities of $ZrTe_5$ and $HfTe_5$ have been measured by adiabatic shield calorimetry from 6 to 350 K on samples carefully shielded to minimize contact between the sample and oxygen during all stages of preparation and measurements. Since $ZrTe_5$ and $HfTe_5$ are isostructural and their molecular volumes almost identical, the small difference between their heat capacities are due essentially solely to mass effects. There is absolutely no indictaion of any excess contribution to

the heat capacities of these compounds below 350 K. The effective thermodynamic dimension of $ZrTe_5$ and $HfTe_5$ is estimated to be between one and two. The molar heat capacity, entropy, and enthalpy at 298.15 K are 18.32 R, 31.96 R, and 4155.7 R·K for $ZrTe_5$, and 18.77 R, 32.99 R, and 4276.8 R·K for $HfTe_5$.

Simon, C.
"Application of Colloid Chemistry in Passive Metal Studies."
Proc., 11th Scandinavian Corrosion Congress, Stavanger 1989. Paper F–16.

The use of colloid chemistry in the study of passive metal electrodes has been found of great interest. The oxide/electrolyte interface has been extensively described on oxide powder suspensions. It is presently extended to the study of oxide covered metal powders in aqueous solution. Surface charge density on such particles and their electrophoretic mobility have been investigated as a function of solution pH.

Simon, C. and Hurlen, T.
"Passive Behaviour of Iron in Alkaline Phosphate Solutions."
Acta Chem. Scand. **43** (1989) 851–854.

Polarization measurements confirm that iron in neutral and alkaline solutions exhibits an essentially potential- and pH-independent stationary passive current. The pH independence may suggest transfer of iron mostly as neutral complex species at the oxide/solution interface. Potentiostatic transients yield initial polarization data which accord with the Cabrera–Mott equation and support z = 2 (rather than 3) for ions being transferred at the metal/oxide interface. Galvanostatic transients yield dc-capacitance data which approach expectations from an exhausted semiconductor model and help to reveal both the mean dielectric constant of the passive film and the main charge distribution in the passive iron electrode under quasistationary conditions. Some differences to the behaviour of passive iron in acidic phosphate solutions are noted.

Stølen, S. and Grønvold, F.
"Thermodynamic Properties of the CuS – Cu_2S System."
Ed. H. Brodowsky og H.–J. Schaller, Kluwer Academic Publishers, Dortrecht, Nederland, 1989, p. 213–220.

The thermodynamic properties of the CuS – Cu_2S system have been studied by means of adiabatic-shield calorimetry in the temperature range 5 to 1000 K. The heat-capacity curves show the prescence of a large number of transitions which have been characterized structurally by powder X-ray and neutron diffraction. A revised phase diagram is presented. The heat capacity data serve as a starting point for evaluation and discussion of the thermodynamic properties of the CuS – Cu_2S system. The calorimeter used for the high-temperature measurements and the experimental procedure are described in detail.

Stølen, S., Fjellvåg, H., Grønvold, F. and Kjekshus, A.
"Thermal Expansion, Compressibility and Heat Capacity of $MnAs_{0.88}P_{0.12}$. A Test of the Chemical Pressure Concept."
Proc. 2nd Asian Thermophys. Prop. Conf., Sapporo, September 1989.

$MnAs_{0.88}P_{0.12}$ takes the hexagonal NiAs-type structure at temperatures above T_D = 460 K and the orthorhombic MnP-type structure at lower temperatures. The gradual deformation of the NiAs-type structure at low temperatures give rise to an anomalously large thermal expansion at 200–500 K, and also to a large, broad peak in the heat capacity. The heat capacity effect is interpreted in terms of a dilational contribution, and its size could be estimated by applying the chemical pressure concept for evaluating the tempera-

ture dependence of the isothermal compressibility. The thus estimated compressibility also shows an anomalous temperature dependence, with higher values at intermediate temperatures. In order to test the applicability of the chemical pressure concept, the temperature dependence of the isothermal compressibility was established experimentally by an equation of state analysis of the measured pressure dependence of the molar volume. It is found that the estimated compressibilities are in good agreement with those experimentally derived.

Velle, O. J., Andersen, A. and Jens, K.–J.
"The oxidative dehydrogenation of ethane by perovskite type catalysts containing oxides of strontium, cerium and ytterbium."
Catalysis Today **6** (1990) 567–574.

Compounds with the general formula $SrCe_{1-x}Yb_xO_{3-0.5x}$ have been characterized by X-ray diffraction (XRD), scanning electron microscope (SEM), temperature programmed reduction (TPR) and BET, and tested for catalytic activity with respect to dehydrogenation of ethane to ethene. XRD indicates that the solubility limit of Yb_2O_3 in $SrCeO_3$ is about 10%, above which a second phase is formed. Furthermore, Yb:$SrCeO_3$ is unstable in the presence of CO_2 as it reacts to $SrCeO_3$ and Yb:CeO_2. TPR measurements indicate that Ce may be reduced from tetra- to the trivalent state. BET measurements yielded specific surface areas of approximately $1 m^2/g$. The different catalyst compositions were tested in a continous flow tubular reactor with two different partial pressures of oxygen at 500, 600 and 700 °C. A maximum yield of 49% was obtained at 700 °C. Possible reaction mechanisms are discussed.

Grønvold, F., Stølen, S. and Svendsen, S. R.
"Heat capacity of α-quartz from 298.15 to 847.3 K, and of β-quartz from 847.3 to 1000 K. Transition behavior and thermodynamic properties."
Thermochim. Acta **139** (1989) 225–243.

The heat capacity of two quartz mineral samples has been measured by adiabatic shield calorimetry in the range 298.15–1000 K. The α–β transition occurs continuously in a λ-like fashion with maximum heat capacity of about 1700 J $K^{-1}mol^{-1}$, over a 0.02 K interval near 847.30 K. The transition enthalpy is 518 ±5J mol^{-1} over a range 820–865 K. The values of molar heat capacity $C_{p,m}$, enthalpy [H_m (1000 K) – H_m (298.15 K)] and entropy [S_m (1000 K) – S_m (298.15 K)] are 69.14 J K^{-1} mol^{-1}, 45633 J mol^{-1} and 75.00 J K^{-1} mol^{-1}, respectively. The results are compared with literature values and a revaluation of the thermodynamic properties of quartz in the range 298.15–1700 K is presented.

Videm, K.
"Corrosion and Selection of Materials for unprocessed Well Fluids."
Int. Conf. Multiphase Flow-Technology and Consequences for Field Development, Stavanger 1989.

Internal corrosion of steels in unprocessed well fluids is described. The guidelines commonly used to predict corrosion rates are far from satisfactory for subsea production and transport lines for oil and gas. Brief descriptions of the many different types of corrosive attack are given. Emphasis is put on giving an understanding of why extensive research so far only has solved some of the complex problems regarding selection of materials for multiphase flow. The report describes various types of carbon dioxide corrosion of carbon steels, discusses problems with sand, small ammounts of hydrogen sulphide and discusses briefly the applicability of stainless steels.

Videm, K. and Dugstad, A.
"Corrosion of Carbon Steel in an Aqueous Carbon Dioxide Environment Part I – Solu-

tion Effects."
Materials Performance vol. 28, 63–67, March 1989.

Corrosion takes place without a corrosion film of ferrous carbonate when ferrous ions are soluble in the environment. The corrosion rate increases proportionally to the carbon dioxide partial pressure to the power of about 0.7. The ammounts of ferrous ions in the water is eqally important as the carbon dioxide level. Low concentrations can leed to rapid corrosion.

When the amounts of ferrous ions exeeds the solubility limit, corrosion films tend to form. Such conditions led to much lower corrosion rates than for solutions with very low amounts of ferrous ions.

Videm, K. and Dugstad, A.
"Corrosion of Carbon Steel in an Aqueous Carbon Dioxide Environment, Part II – Film Formation."
Materials Performance vol. 28, 46–50, April 1989.

These experiments were performed to achieve better insight into the corrosion phenomena occuring in the water phase of a gas pipeline with liquid drop out and no formation water. When corrosion rates are predicted from experiments where corrosion films do not form, the rates tend to be much too high. To improve the situation, the first aspect is to clarify under which conditions films form and then understand their protecting properties.

Videm, K. and Dugstad, A.
"Galvanic Influence of CO_2-Corrosion."
NACE Corrosion/89, p. 468.

Galvanic acceleration of internal corrosion of carbon steels in gas- and oil well environments can occur because dissimilar metals are coupled together, when protecive films are locally destroyed by turbulent flow or particle erosion, or when concentration gradients occur in the environment due to deposits. Electrochemical experiments have been carried focused on finding out under which conditions galvanic effects contribute to make corrosion severe and when they do not.

Stainless steels obtain well insulating films in aqueous carbon diaxide environments and will often not create severe problems when coupled to carbon steels. But conditions were found where margins were small towards induction of pitting of the carbon steel. Carbon steels even of nominally the same type can be rather dissimilar. Corrosion problems created by this are forcast to be severe in some cases.

Videm, K. and Dugstad, A.
"Predicting CO_2-Corrosion in Oil and Gas Well Environments."
Proceedings 11th European Corrosion Congress, Utrecht, 1989, p. 48.

The rules for predicting carbon dioxide corrosion of carbon steel used by most oil companies do not take care of the composition of the formation water and the fact that carbon dioxide corrosion is a family of different types of attack rather than a single phenomenon. The paper gives guidelines for how better predictions can be made. However, in many cases data are not awailable for giving more than semiquantitative forcasts.

Videm, K. and Dugstad, A.
"The Many Facets of CO_2-Corrosion of carbon steel."
Proceedings 11th Scandinavian Corrosion Congress, Stavanger 1989, Paper F–62.

Aqueous carbon dioxide corrosion of carbon steel in oil- and gas well environments is a family of different types of attack rather than a single phenomenon. It is essential to realize this because the response of the corrosion rate to a variable is different for the various types of corrosion. The report treats corrosion film

formation, rate of penetration as a function of carbon dioxide partial pressure, flow rate and pH for attack without ferrous carbonate films, the influence of protective films, sand effects and attack by condensation.

Videm, K. and Dugstad, A.
"Radioactive and Electrochemical Techniques for Corrosion Monitoring."
Proc. 11th Scandinavian Corrosion Congress, Stavanger 1989, Paper F–78.

Making materials radioactive and determine the loss of metal as a function of time by measuring the corresponding reduction in radiation intensity, is an accurate and reliable method for determining corrosion rates. The paper describes experience with this technique, different alternatives for activation, instrumentation and probes. In-situ electrochemical methods are described. It is recommended to use polarization just outside the linear region. A method for treating the data without a computer is presented. Combined use of electrochemical and radioactive techniques are finally discussed.

Wilhelmsen, W.
"Electron Transfer Reactions of Titanium(III)/(IV) on Passive Titanium."
Acta Chem. Scand. **43** (1989) 345–350.

The electron transfer reactions of titanium (III)/(IV) at passive titanium electrodes have been studied by transient polarization measurements at various values of the passive film thickness and concentrations of the redox couple. The Tafel curves for the redox reactions are complex. The anodic curve exhibits two linear regions, and the cathodic curve is non-linear below –0.2 V(sce). Near the reversible Ti(III)/(IV) potential, however, the Tafel curves are linear with cathodic transfer coefficient near 1 and anodic transfer coefficient near 0, and they extrapolate to a common value of the exchange current at this potential. In this overvoltage region, the electron transfer is nearly independent of the film thickness. At higher anodic overvoltages, both the anodic current and transfer coefficient decreases with increasing film thickness. The polarization data indicate electron exchange with the conduction band of the passive film. The oxidation of Ti(III) appears to have the $TiOH^{2+}$ ion as the main electroactive species. The rate of electron transfer is found to be first order in reactant dependence, and to depend strongly on the nature of the electrolyte.

Yang, Z. J., Bratsberg, H., Johansen, T. H., Norman, N., Taftø, J., Lorentzen, L., and Skjeltorp, A. T.
"The effect of Pb-doping in Bi–Sr–Ca–Cu–O and Sb-doping in Bi–Pb–Sr–Ca–Cu–O superconductors."
Physica C submitted.

A series of samples with nominal starting compositions $Bi_{1.4}Pb_{0.6}Sr_2Ca_3Cu_4O_z$ and $Bi_2Pb_{2x}Sr_2Ca_3Cu_4O_z$ ($0.1 \leq x \leq 0.4$) were prepared using dry and wet methods. X-ray emission studies of SEM and TEM show that most of the Pb-doping is lost during sintering, but Pb apparently acts as catalyst to form the high-T_c phase. Another series of samples with starting compositions $Bi_{2(1-x)}Pb_{2x(1-y)}Sb_{2xy}Sr_2Ca_3Cu_4O_z$ ($0.2 \leq x \leq 0.3$ and $0.2 \leq y \leq 0.7$) and $Bi_{2(1-x)}Pb_{2x}Sb_{2y}Sr_2Ca_3Cu_4O_z$ ($0.2 \leq x \leq 0.3$ and $0.03 \leq y \leq 0.08$) were prepared by the wet method. Susceptibility measurements indicate a range of Sb-doping levels producing a well developed high-T_c phase. The superconducting transition of Sb-doped Bi–Pb–Sr–Ca–Cu–O specimens is very sensitive to the strength of a.c. measurement fields and external d.c. fields.

❑

Research partners outside the University of Oslo

Norway

Institute for Energy Technology, 2007 Kjeller (A. F. Andresen, O. Steinsvoll, A. Dugstad, L. Lunde, W. Wilhelmsen; neutron scattering, magnetic materials, corrosion, electrochemistry).

Center for Industrial Research, Oslo 3 (R. Bredesen, K. -J. Jens, T. Briseid, G. Eidså, B. Thorstensen, A. Andersen; thin superconducting films, oxides for CO oxidation, bacterial corrosion, fuel cells, methane conversion).

University of Trondheim (NTH), Trondheim (S. Julsrud, R. Tunold, Ø. Johannesen; thermodynamics, electrochemical reactors).

Norsk Hydro, Oslo (T. Søntvedt; corrosion).

Sweden

University of Uppsala (L. Häggström; Mössbauer-spectroscopy).

Denmark

University of Aarhus (A. N. Christensen; powder diffraction).

University of Odense (P. Norby; structure of zeolites and silicates).

Risoe National Laboratory, Roskilde (B. Lebech; neutron diffraction).

Germany

Max Planck Institut für Festkörperforschung, Stuttgart (A. Simon, H. –G. von Schnering, W. Hönle, W. Bauhofer; crystal growth, low-dimensional materials, phase transitions, cluster compounds).

Phillips Universität, Marburg (U. Sondermann; magnetic materials).

Physikalisches Institut, Göttingen (K. Bärner; magnetic materials).

Gesamthochschule Paderborn (T. Krüger; high pressure studies).

Hasylab, Hamburg (M. Nielsen; powder diffraction, EDS).

England

University of Birmingham, Birmingham (F. J. Berry; Mössbauer-spectroscopy).

France

Université d`Aix-Marseille II and I (Y. Mathey, J. P. Sorbier; low-dimensional materials, conductivity).

Institut Laue Langevin, Grenoble (M. S. Lehmann, C. Vettier; neutron scattering).

Elf Aquitaine, Pau (J. L. Crolet; corrosion).

Poland

Academy of Mining and Metallurgy, Krakow.

University of Krakow (A. Zieba, R. Zach; magnetic materials, pressure induced transitions).

U.S.S.R.

Vernadsky Institute of Geochemistry and analytical Chemistry, Academy of Sciences, Moscow (I. L. Khodakovsky; CODATA – International Chemical Thermodynamic Tables).

U. S. A.

University of Michigan, Ann Arbor (E. F. Westrum, R. Shaviv; heat capacity).

Chemical Thermodynamics Division, US National Institute of Standards and Technology (D. Garvin; CODATA – International Chemical Thermodynamic Tables).

Brazil

University of Sao Paulo (C. C. Beccerra, N. F. Oliveira; phase diagrams, critical phenomena).

❑

Personnel

In 1989, the Section for Inorganic Chemistry had

9 scientists employed by the Department of Chemistry,
6 scientists employed through funds from external sources,
8 engineers and technicians,
9 doctorate students and research fellows,
11 graduate students.

The following abbreviations will be used below:

UiO	University of Oslo.
SI	Center for Industrial Research, Oslo.
IFE	Institute for Energy Technology, Kjeller.
NTH	Norwegian Institute of Technology, Trondheim.
NTNF	Royal Norwegian Council for Scientific and Industrial Research.
NAVF	Royal Norwegian Research Council for Science and Humanities.

Permanent scientific staff

Helmer Fjellvåg (35), senior lecturer.
Cand. real. from UiO in 1978. Head of the Section for Inorganic Chemistry in 1989. Teaches general and inorganic chemistry and solid state chemistry. Area of research: Structural and physical properties of transition metal compounds, oxides and silicates; metallization of semiconductors; synthesis; powder diffraction (PXD, PND, SR).

Sigrid Furuseth (50), senior lecturer.
Cand. real. from UiO in 1964. Teaches general and inorganic chemistry. Area of research: Synthesis, structure determination and characterisation of inorganic compounds with emphasis on low-dimensional structures.

Fredrik Grønvold (65), professor.
Master of Science at the University of Michigan in 1951. Teaches inorganic chemistry, thermodynamics and materials science. Area of research: Thermodynamic, structural, and magnetic properties of inorganic compounds.

Arne Kjekshus (57), professor.
Dr. philos. at the University of Oslo in 1970. Teaches general and inorganic chemistry. Area of research: Synthesis and characterisation of inorganic compounds – superconductors, semiconductors, and magnetic materials.

Per Kofstad (60), professor.
B.A. from Pomona College, California in 1950 and Ph. D. from University of California, Berkeley in 1953. Dr. philos at UiO in 1964. Teaches inorganic chemistry and solid state chemistry. Area of research: high temperature corrosion and ceramic materials. Appointed head of the newly established Center for Materials Research in the Research Park located next to the University at Blindern.

Trond Rakke (45), senior lecturer.
Dr. philos. at UiO 1980. Teaches general and inorganic chemistry and materials science. Area of research: Properties of pnictides and chalcogenides.

Erling Røst (65), senior lecturer.
Cand. real. from UiO in 1955. Teaches general and inorganic chemistry. Area of research: Structure and phase relations in inorganic compounds and systems.

Sven R. Svendsen (63), senior lecturer.
Cand. real. at UiO in 1954. Teaches general and inorganic chemistry. Area of research: Thermodynamic properties of inorganic compounds.

Ketil Videm (57), professor.
Ph. D. in Physical Metallurgy at NTH in 1974. Teaches materials science, electrochemistry, and corrosion. Area of research: Aqueous electrochemistry and corrosion of metals.

Other scientific personnel

Per Hagerup Andresen (30), research fellow (NAVF).
Cand. scient. at UiO in 1987. Area of research: Synthesis and characterisation of superconducting oxides.

Espen Bergsmark (29), scientist (NTNF).
Cand. scient. at SI/UiO in 1988. Area of research: Oxide-based cathode materials and other materials for solid oxide fuel cells.

Orvar Braathen (72), visiting scientist (project).
Previously Managing Director of Megon a/s. Works with synthesis of ceramic superconductors.

Scientists employed by the Department of Chemistry and scientists employed through funds from external sources from left to right: Tor Hurlen, Sigrid Furuseth, Pavel Karen, Per Hagerup Andresen, Fredrik Grønvold, Helmer Fjellvåg, Trond Rakke, Erling Røst, Espen Bergsmark and Sven R. Svensen.

Tor Hurlen (63), professor (NAVF).
Cand. real. 1952, Dr. philos. 1964. Area of research: Aqueous electrochemistry and corrosion of metals.

Alexander Kapitan, scientist (UD/NAVF), Ukraina, U.S.S.R.
Spent 10 months in 1989 at UiO, cultural exchange fellow with the Soviet Union. Area of research: Metallization of GaAs; the ternary Co–Ga–As system.

Pavel Karen (38), scientist (NAVF).
Ph. D. in inorganic chemistry from Prague 1984. Area of research: Studies of chemical, phase properties of ceramic high-T_c superconductors and relations between their structure and electrical properties.

A. S. Khanna (37), scientist (Post-Doc. Fellow/NTNF).
Ph. D. in metallurgical engineering at Madras University, India in 1985. Area of research: High temperature corrosion.

Poul Norby (30), research fellow (Carlsberg-foundation/NTNF).
Cand. scient. from Aarhus University in 1986. Visiting fellow at UiO in the period 1987–89. Ph. D. dissertation in 1989: "Synthesis and structural investigations of zeolites and related alumino silicates."

Truls Norby (34), scientist (NTNF).
Dr. scient. 1986 at UiO. Area of research: High-temperature electroceramics for electrochemical reactors; oxides with ionic (oxygen ions and protons) or electronic conductivity.

Andrzej Zieba, scientist (NAVF, three months yearly at UiO).
Dozent at Academy of Mining and Metallurgy, Krakow. Area of research: Magnetic materials, pressure induced transitions, multicritical behaviour.

Technical staff

Kari Bjerkelund (51), engineer.
Operation of instruments for thermoanalytical and magnetic measurements, and operation of X-ray diffraction instruments.

Oddvar Dyrlie (32), (Norsk Hydro/NTNF).
Engaged to work with fabrication and characterisation of oxide ceramics, and measurements of proton conductivity in oxides.

Per Fostervoll (44), engineer.
Operation of instruments for different X-ray diffraction methods as well as the new SQUID instrument.

Ole Jakob Kjørstad (20).
Laboratory technician for student laboratory courses.

Ingvild Lorentzen (24), engineer. (NTNF/NAVF/UiO).
Operation of the Auger/XPS instrument and the Scanning Electron Microscope.

Bjørn Lyng Nielsen (67).
Operation and maintenance of calorimetric instruments.

Hege Lynne (32).
Works as laboratory technician in student laboratory courses.

Bjørg Osvik (35).
Technical lecture assistant in the main auditoriums.

Doctorate students and their subject titles

Egil Gulbrandsen (32), research fellow.
Cand. scient. at UiO in 1987. "Electrochemistry and corrosion of magnesium and other light metals."

Lill Halvorsen (27), research fellow (SI/NTNF).

Chemical engineer (M. Sc.) at NTH 1987.
"Ion conduction in ceramic oxides."

Arve Holt (28), research fellow (Elkem/NTNF).
Cand. scient. at UiO in 1987. "Transport processes in ceramic materials in connection with high temperature corrosion and of effects of carbon and hydrogen on properties of ceramics".

Ingvill Hornkjøl (25).
Cand. scient. from UiO in 1988. "An investigation of the passive-active transition of titanium, and its consequences for hydrogen evolution and absorption."

Sverre Hornkjøl (28), research fellow.
Cand. scient. at UiO in 1986. "Passive behaviour of zirconium, hafnium, and niobium."

Karin H. E. Loftsgaard (29), research fellow.
Cand. scient. at UiO in 1988. "Structural and phase-related investigations of oxides; the Bi–K–Cu–O system."

Ole Jacob Velle (31), research fellow (Saga/SI/NTNF).
Chemical engineer (M. Sc.) from NTH 1984.
Process engineer in Saga Petroleum a/s.
"Electrochemical conversion of natural gas."

Graduate students and their subject titles

Jorunn Fjellstad Schjerven (24).
"Structure and properties of phases in the system Ni–Ga–As."

Doctorate students,engineers and technicians from left to right: Sverre Hornkjøl, Hege Lynne, Egil Gulbransen, Lill Halvorsen, Kari Bjerklund, Oddvar Dyrlie, Per Fostervold, Ingvild Lorentzen, Karin Loftsgaard and Arve Holt.

Rita Glenne (24).
"Effect of substitution on structure and superconductivity properties in $YBa_2Cu_3O_{9-\delta}$."

Bente Gilbu Hømandberg (24).
"Characterisation and low-temperature oxidative degradation of low-dimensional hafnium telluride." Graduated November 1989 and proceeds with the doctorate degree.

Lisbeth S. Jakobsen (31).
"Electrical conductivity in oxides; Calcia-doped ytterbia."

Anne Johansen (23).
"Passive behaviour of beryllium."

Ole Bjørn Karlsen (28).
"Investigations of the ternary system Au–Cu–Sn."

Yngve Larring (23).
"Proton conduction in oxides; Calcia-doped yttria." Also works as laboratory assistant in student courses.

Aud H. Larsen (25).
"Vanadate induced corrosion of iron." Graduated 1989.

Tove Navestad (25).
"Vanadate induced corrosion of nickel." Graduated 1989.

Per Arne Osborg (26).
"Electrical conductivity in ternary oxides."

Heidi Thoresen (26) (SI/UiO).
"Computer calculation of the Mg–Fe–Mn phase diagram."

❑

Graduate students from left to right: Ingvild Hornkjøl, Anne Johansen, Truls Norby (scientist), Rita Glenne, Yngve Larring, Lisbeth Jacobsen, Per Arne Osborg and Bente Gilbu.